FAR INFRARED OPTICAL ABSORPTION IN MANGANESE FLUORIDE

FAR INFRARED OPTICAL ABSORPTION IN MANGANESE FLUORIDE

by

JOHN NEIMANIS, B.Sc.

A Thesis
Submitted to the Faculty of Graduate Studies
in Partial Fulfilment of the Requirements
for the Degree
Master of Science

McMaster University
May 1971

MASTER OF SCIENCE (1971)
(Physics)

McMASTER UNIVERSITY
Hamilton, Ontario

TITLE: Far Infrared Optical Absorption in Manganese Fluoride

AUTHOR: John Neimanis, B.Sc. (McMaster University)

SUPERVISOR: Dr. T. Timusk

NUMBER OF PAGES: vi, 47

SCOPE AND CONTENTS:

The optical absorption in manganese fluoride has been studied in the range of 30 to 300 cm^{-1} with emphasis placed on the possible multiple magnon absorptions (other than two-magnon) and an induced single magnon absorption. It is shown that theoretically one can expect four-magnon processes by expanding the Heisenberg spin hamiltonian to higher orders in the creation and annihilation operators introduced by the Holstein-Primakoff transformation. However, neither an induced one magnon nor four magnon process was observed. The absorptions which were seen in the spectra were attributed to phonon processes.

ACKNOWLEDGEMENTS

It is with great pleasure that I thank my supervisor, Dr. T. Timusk, for his encouragement and help throughout the course of this work. Dr. D. Goodings' clarification of the theoretical aspects of magnetism has been very valuable. Most of all I would like to express my appreciation to Ralf Kuehnel for the crystals and Roger Ward and Adrian Tumber for their assistance in developing the interferometer system.

This research was partially funded by the Defense Research Board of Canada. I am also grateful to the National Research Council of Canada for the award of a fellowship.

Finally, I thank Mrs. S. McQueen for typing the final manuscript.

TABLE OF CONTENTS

LIST OF FIGURES

CHAPTER I

INTRODUCTION

Manganese fluoride has undergone considerable investigation in recent years because it is one of the simplest antiferromagnets to treat theoretically. Of particular interest have been the results of local magnon mode experiments as reported by Weber[1] and by Buyers et al.,[2] of two-magnon absorption as reported by Allen et al.[3], and inelastic neutron measurements to determine the magnon dispersion curves by Low et al[4] and others.[5] Variation of the frequency of the zone boundary magnons with temperature has been reported by Turberfield et al.[6] with emphasis placed on the nature of the excitations near the Neel temperature. Phenomenological theories describing the two-magnon process have been developed by Allen et al.,[3] Loudon,[7] Elliott[8] and Thorpe, and other workers.[9,10]

In the present work an attempt is made to observe an induced one-magnon absorption in doped crystals of MnF_2 and multiple magnon processes (other than two-magnon) in pure MnF_2. The experimental apparatus and sample preparation are discussed in Chapter II. In Chapter III, the possibility of four-magnon processes are derived using the Heisenberg spin hamiltonian as proposed by Loudon.[7] The results are presented in Chapter IV and it is significant that within the limits of the present experimental setup, no one-magnon or multiple-magnon processes are observed. However phonon absorptions do appear throughout the range of the experiment (from 30 to 300 cm^{-1}). These are analyzed with respect to polarization and origin. It is important that the phonon absorptions are well known so that one is able to distinguish magnetic effects apart from these.

CHAPTER II

EXPERIMENTAL APPARATUS AND TECHNIQUE

(a) Equipment

The experiments were performed using a commercial far infrared Michelson interferometer (RIIC FS-720) which has been modified to provide a double beam signal. The top half of the beam is used as a standard and is not incident on the travelling mirror in the interferometer. It is reflected from a fixed mirror shadowing the upper half of the movable mirror. Adjustment of the mirrors allows one to obtain a null signal of the desired frequency at the detector when the travelling mirror is well removed from the position of zero path difference. The actual signal at the detector is composed of one half from the standard beam and the other half from the interfering beam 180 °out of phase. The lock-in amplifier gives the difference between these two signals yielding zero at the output. It was not possible to regulate the high pressure mercury lamp (Phillips HPK 125W) to better than 1% fluctuations in both the visible and far infrared regions by other means. The double beam operation reduces these changes to less than 0.05% of the maximum signal size at the detector.

The spectral region from 10 to 625 cm^{-1} may be scanned with this interferometer although the high frequency region beyond 400 cm^{-1} is inaccessible due to lack of a proper filter system. An acceptable filter combination for the present high frequency work consisted of a black polyethylene membrane at the exit from the interferometer, at room temperature, and a liquid-helium-temperature sapphire window above the detector. The black polyethylene eliminates all chopped radiation from the source at higher frequencies than can be sampled by the pulse system. Most of the room temperature background radiation is absorbed by the sapphire. Room temperature measurements with a Beckman IR-12 spectrometer showed sapphire absorbs in the region 300 to 1350 cm^{-1}. The black polyethylene and sapphire together transmit less than 0.5% from 300 to 1500 cm^{-1}. At helium temperature the absorption band in the sapphire becomes narrower as evidenced by runs done only with the filters. Here the intensity of the spectrum decreases steadily from a maximum at 150 cm^{-1} to about 15% at 300 cm^{-1} and 5% at 350 cm^{-1}. Above this frequency the signal to noise ratio of the spectrum is too large to make acceptable measurements.

The light pipe and sample holder are shown in figures 1 and 2. The sample chamber must be electrically isolated from the interferometer. This is accomplished by a nylon coupling joining the light pipe to the interferometer and a thin mylar vacuum window glued at the entrance to the light pipe. Radiation travels down the polished brass pipe, through a long cone containing the sample, and is incident on the detector assembly.

Figure 1

Top section of sample chamber showing connection to interferometer, light pipe elbow, and gate valve assembly. The mylar window provides electrical insulation from the interferometer and a vacuum seal. The gate valve allows changing the sample without retransferring liquid helium.

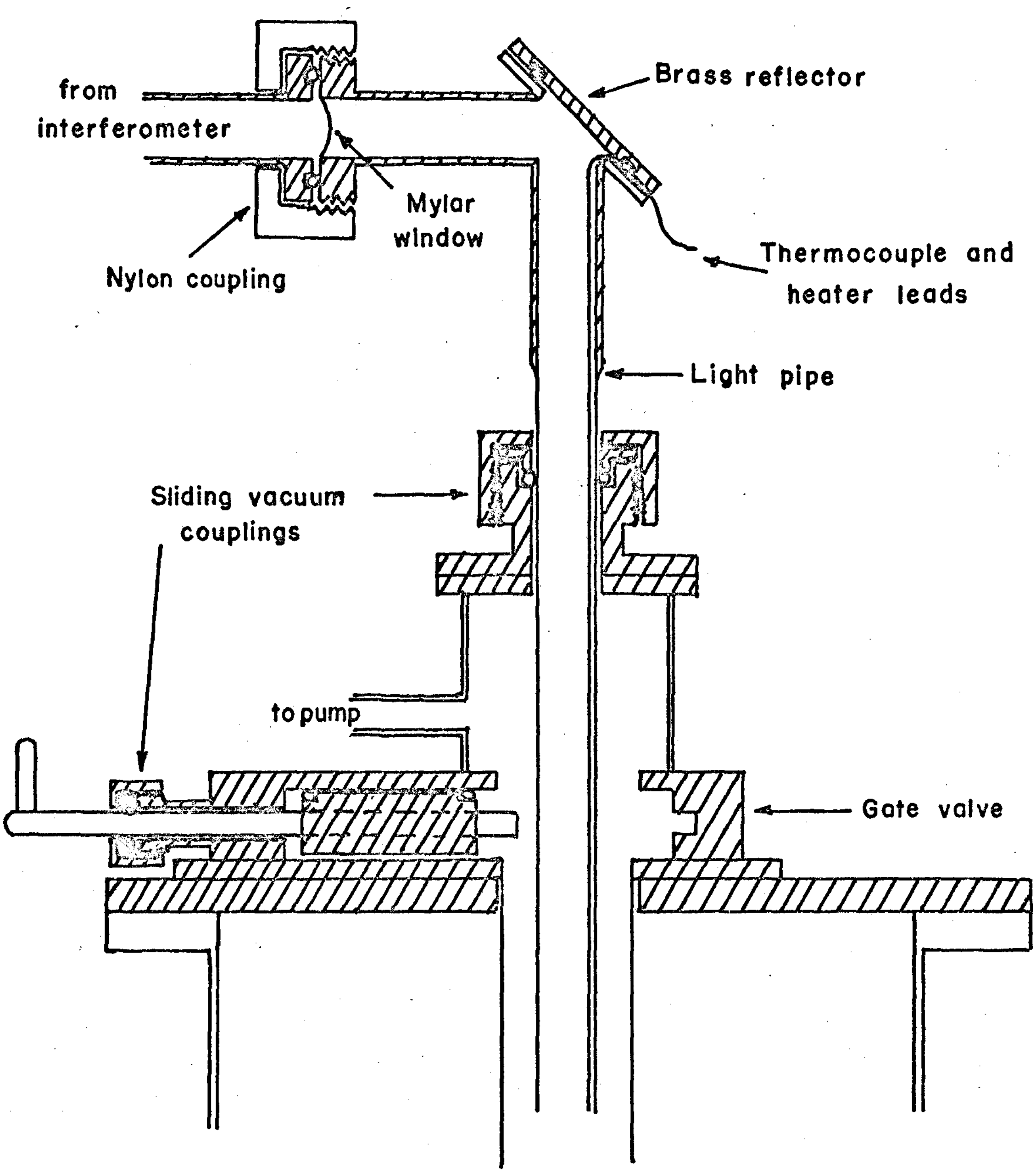
from
interferometer
Brass reflector
Mylar
window
Nylon coupling
Thermocouple and
heater leads
Light pipe
Sliding vacuum
couplings
to pump
Gate valve

Figure 2

Bottom section of sample chamber showing position of superconducting solenoid. Note the long cone for focussing radiation onto the detector.

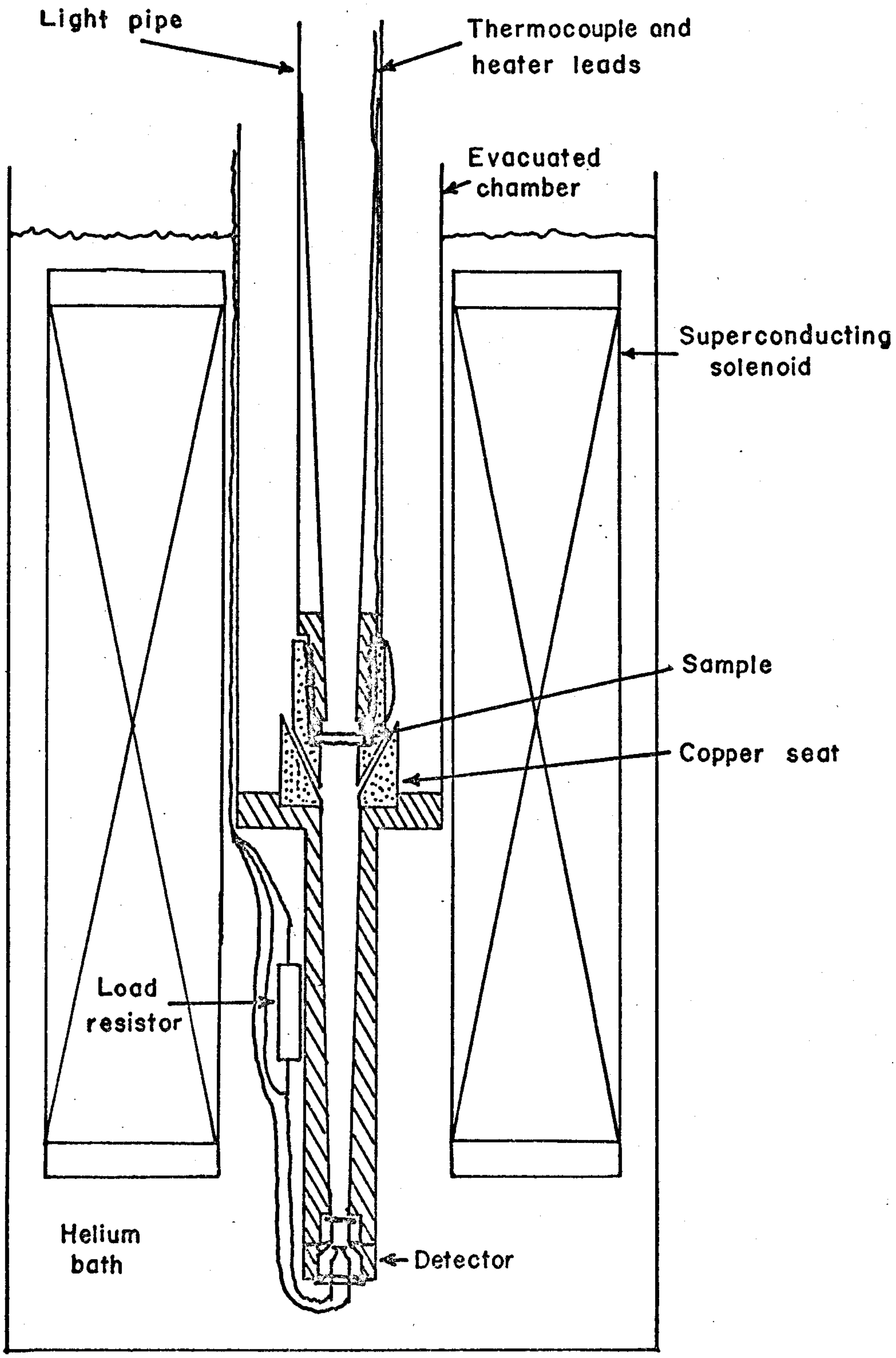
Light pipe
Thermocouple and heater leads
Evacuated chamber
Superconducting solenoid
Sample
Copper seat
Load resistor
Helium bath
Detector

The long cone condenses the light to the size of the detector and minimizes the number of rays reflected back up the light pipe. The detector is a liquid-helium-cooled, gallium-doped, germanium bolometer having a resistance of about 300 kilohms at 4.2°K. The leads are soldered to the element with indium in a reducing hydrogen atmosphere and this improves the noise characteristics of the detector compared to those which had been used previously.[11]

The gate valve enables one to remove the light pipe and sample from the chamber, exchange samples, and re-insert the light pipe without retransferring liquid helium. In practice it was found that this process caused about a litre of helium to boil off. The use of exchange gas and a slower insertion, thereby allowing the light pipe to reach thermal equilibrium gradually, could possibly reduce the helium loss to a third of a litre. When experiments were performed without the superconducting magnet, an inner glass dewar with 2 1/2 litres capacity was utilized to minimize helium requirements and hence changing of samples without retransferring helium was not feasible. However, with the magnet dewar, the capacity is about 10 litres and it is important to be able to change samples without having to remove the complete sample chamber.

With the sample chamber in position, the detector is level with the bottom end of the solenoid. A 50 kilogauss field at the centre of the magnet increases the resistance of the bolometer by about 10%. However, no adverse performance characteristics of the bolometer were noticed and the use of magnetic shielding was considered unnecessary. With the magnet power supply off the RMS signal-to-noise ration on the interferogram was about 600. The electrical noise from the power supply reduces the ratio to about 400. Increasing the field to the maximum of 60 kilogauss further reduces the ratio to about 300. This latter noise increase is attributed to the higher rate of helium boil-off which causes mechancial vibrations of the detector.

The thermocouple and heater leads pass through an epoxy seal in the elbow and down the inside of the light pipe. A 100 ohm Allen Bradley miniature carbon resistor at the junction of the sample holder and light pipe is effective in heating the sample to about 100°K. The thermocouple passes through a small hole in the side of the sample holder and is in contact with the sample. The chromel vs. gold .02% iron thermocouple was calibrated from 4.2 to 20°K using a germanium resistance thermometer and from 20 to 100°K with a standard copper-constantan thermocouple. Readings were taken with a Hewlett-Packard model 3420B differential voltmeter which has an upper sensitivity of 0.2 microvolts. The temperature variation during runs was less than 1°K in the range 4.2 to 20°K and less than 2°K above that. At helium temperatures the thermocouple reading was constant to one microvolt (about 0.1°K).

Although the light pipe is machined down to .015 inches wall thickness, there is still considerable heat conduction to the helium bath if the sample chamber is evacuated. This necessitates the use of helium exchange gas for experiments at 4.2°K. About 250 microns of helium gas in the sample chamber is sufficient to cool the samples to 4.2°K and minimize liquid helium boil-off. The performance of the bolometer deteriorates to an unacceptable level in the presence of exchange gas because of the high thermal conductivity of the gas. Figure 3 shows a simple method of isolating the bolometer from the sample chamber. The epoxy (Emerson Cuming Inc. Stycast 2610 GT) used to hold the sapphire filter to the thin wall of the brass bolometer holder will not crack at helium temperatures. Differential thermal expansion is not a problem because the .010 inches thick brass flexes enough to maintain the seal. The air inside the cavity is frozen to the walls of the holder when liquid helium is transferred into the dewar and the bolometer is thus under vacuum. Mounting the cold filter immediately above the bolometer ensures that the filter remains close to 4.2°K even during the high temperature runs. The absorption characteristics of the filter are not altered and variations with temperature in the spectra are attributable directly to the change in temperature of the sample being studied. The detector holder has been cycled from 300°K to 4.2°K about a hundred times without adverse effects.

Figure 3

Detailed view of detector holder. The epoxy (Stycast 2610 GT) provides an effective vacuum seal at liquid helium temperatures.

Figure 4

Circuit to provide reference signal for lock-in amplifier. The reversing switch at the input changes the phase at the output by 90°. The set or clear buttons on the counter change the phase by 180°. The resistors provide almost 180° sweep in the phase.

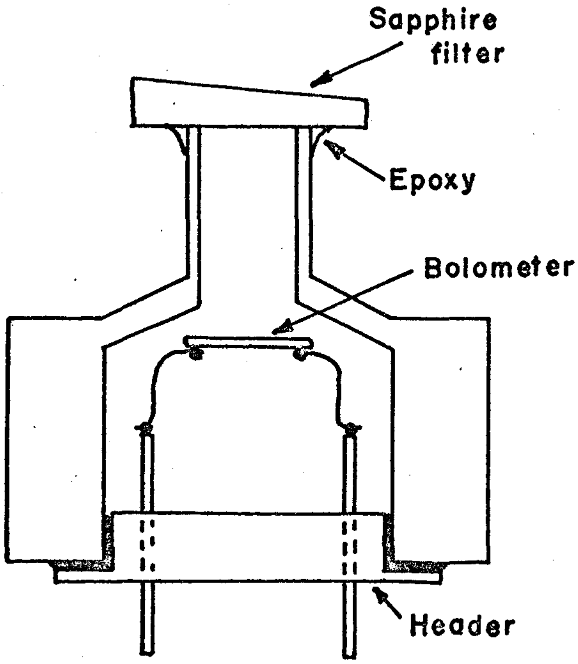
Sapphire filter
Epoxy
Bolometer
Header

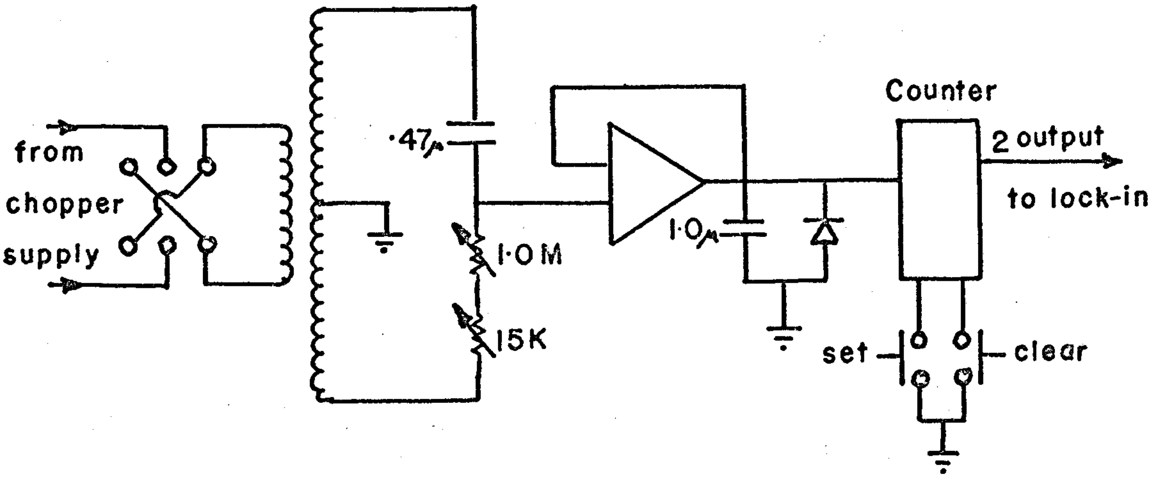
from chopper supply
·47μ
1·0M
15K
1·0μ
Counter
2 output
to lock-in
set
clear

A block diagram of the experimental layout is given in figure 5. The reference signal for the phase sensitive detector is supplied by the phase shifter of figure 4. A variable frequency amplifier drives the synchronous chopper motor which is designed to run at 1800 rpm with a 60 cps supply. The transformer is in parallel with the chopper motor. Changing the resistance in the secondary from zero to infinity causes a phase shift of 180° in the signal between the centre tap of the transformer and the input of the operational amplifier (Zeltex Inc. Model ZEL-1). The amplitude of this signal remains at a constant 10 volts peak-to-peak. Phase shifting properties of the RC network are not affected by the high input impedance of the operational amplifier and, in practice, a shift of about 170° is obtained for the range 100 to 10^6 ohms. The desired signal frequency is half of the chopper supply frequency and the divide-by-two output of the binary counter (Motorola MC839P) provides this. The reversing switch at the transformer input and the set and clear buttons for the counter provide phase shift of 90° and 180° respectively at the output.

The Moire grating in the interferometer produces fringes every 8 microns, or 16 microns path difference. Amplification and selection of these fringes is accomplished by the circuit shown in figure 6. If the interferogram is sampled at every fringe the maximum frequency of signal radiation which can be unambiguously resolved is 1/16 microns or 625 cm^{-1}. Since not all of the spectra studied extended to this frequency

Figure 5

Block diagram of experimental equipment used for producing and recording interferograms. The oscilloscope and pen recorder are used to monitor signal noise during a run.

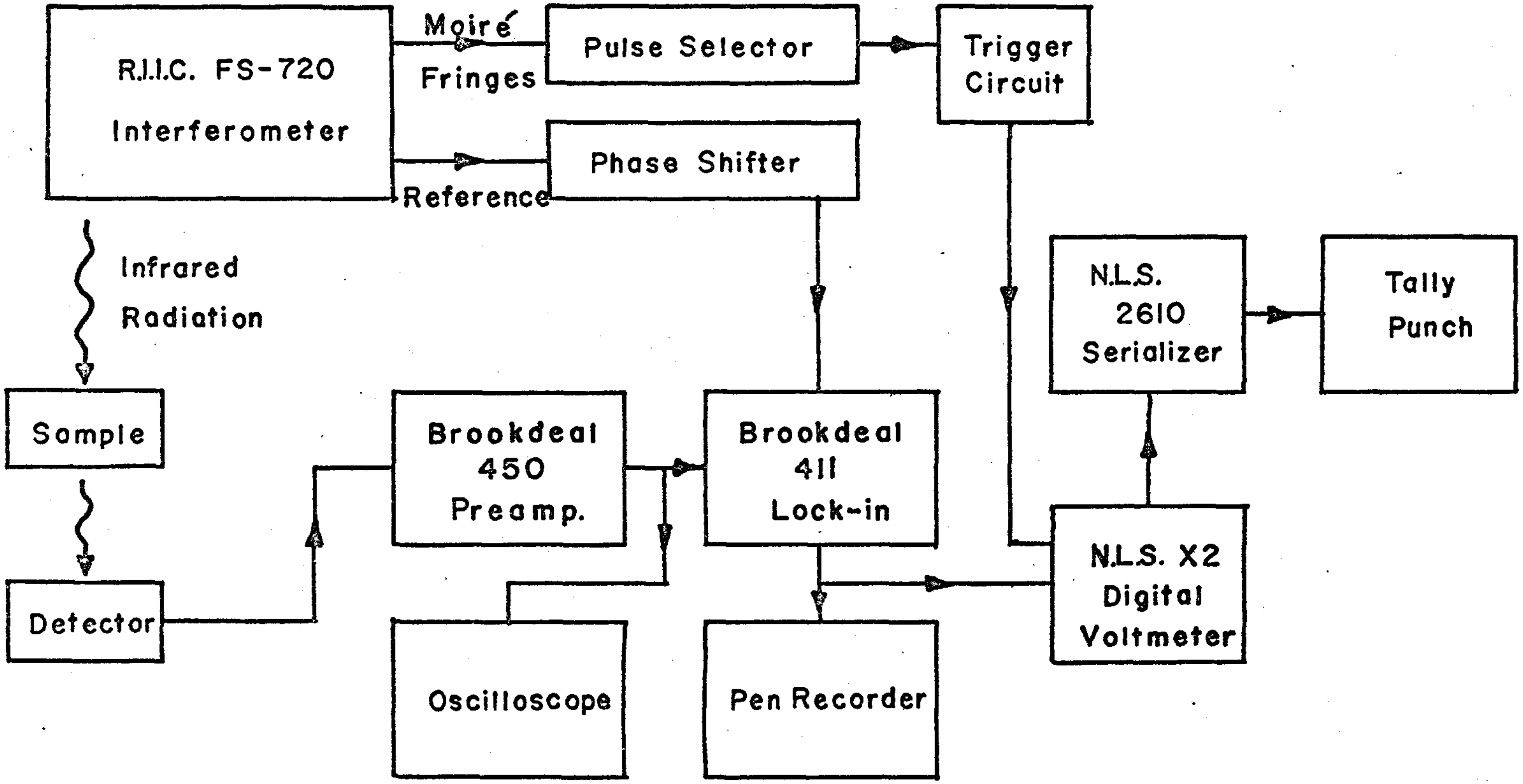
R.I.I.C. FS-720
Interferometer
Moiré
Fringes
Reference
Pulse Selector
Phase Shifter
Trigger
Circuit
Infrared
Radiation
Sample
Detector
Brookdeal
450
Preamp.
Brookdeal
411
Lock-in
Oscilloscope
Pen Recorder
N.L.S.
2610
Serializer
Tally
Punch
N.L.S. X2
Digital
Voltmeter

Figure 6

The Moiré fringe signal amplifier and selector circuits. The capacitor and resistor combination at the monostable multivibrator delay the pulses to the counter if desired. The binary outputs determine the range of spectral radiation which may be detected during any run.

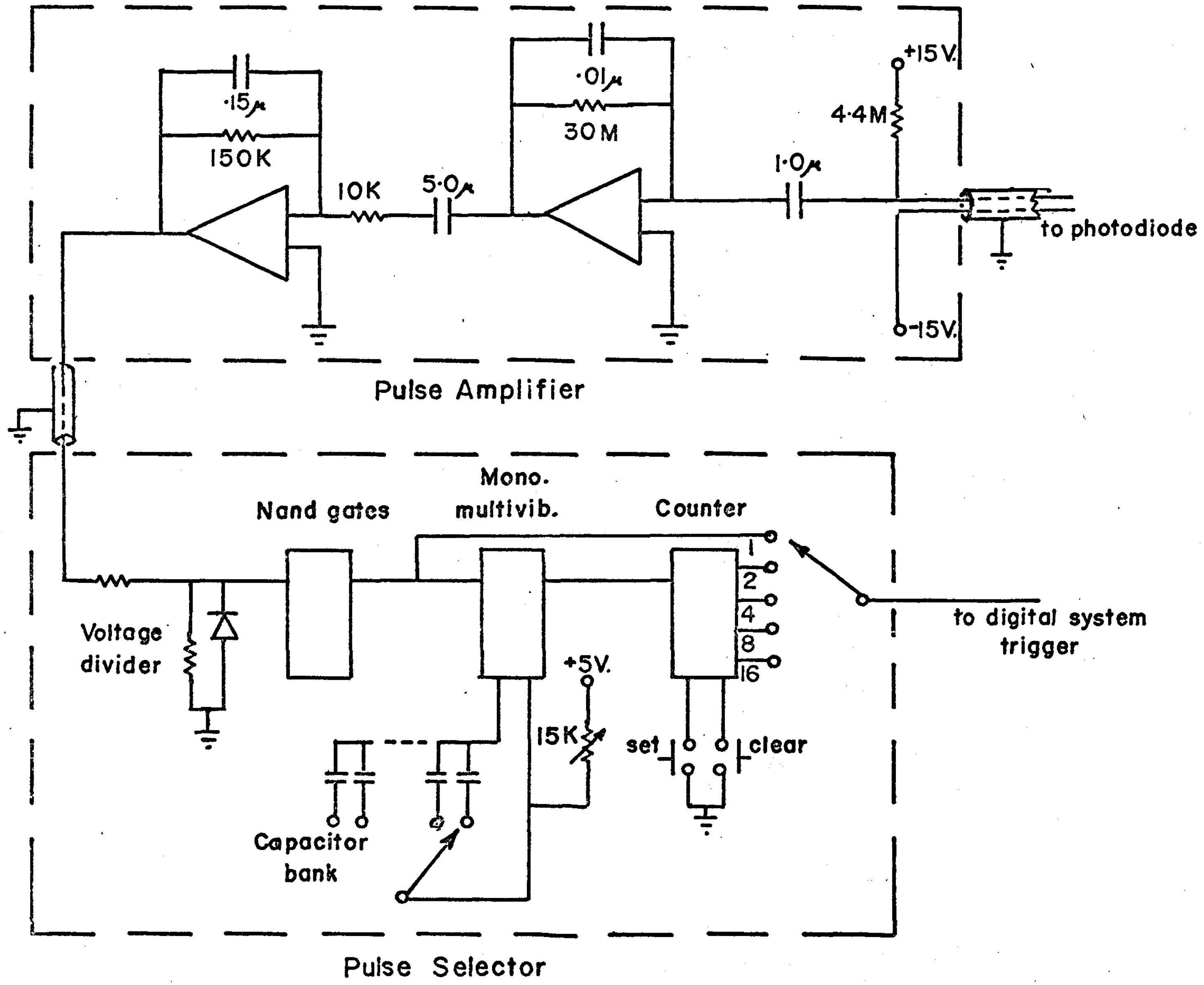
·15µ
150K
10K
5·0µ
·01µ
30M
1·0µ
+15V.
4·4M
to photodiode
-15V.
Pulse Amplifier
Mono. multivib.
Nand gates
Counter
1
2
4
8
16
to digital system trigger
Voltage divider
+5V.
15K
set
clear
Capacitor bank
Pulse Selector

limit it is desirable to be able to sample the interferogram at 16, 32, 64, or 128 microns giving upper frequency limits of 312.5, 156, 88, and 44 cm^{-1} respectively thereby saving on running time for the experiment computer time for the transforms.

A d.c. light source is focussed through the Moire grating onto a photodiode (Texas Instruments IN 2175). A 4.4 megohm load resistor was found to approximately zero the d.c. voltage level at the input to the amplifier. The 1.0 μfd capacitor removes any remaining d.c. level. A sine wave signal of 0.3V peak-to-peak around zero is thus fed into the first amplification stage. As well as being an impedance matching device, the first stage eliminates most of the 60 cps pickup in the system and amplifies the signal to about 8 volts peak-to-peak. The second amplifier stage is driven to saturation producing an almost square wave input to the pulse selector. The two amplifier stages are capacitatively coupled to ensure only that portion of the signal immediately about the zero level is used for the triggering. Zero drift at the output of the photodiode was found to be of the order of the Moiré signal size over the full range of mirror travel. Both halves of the square wave at the amplifier output are of equal duration indicating long term drifts on the fringe signal have been eliminated.

The amplifier output signal is passed through a voltage divider and a clipping diode to produce a 0 to 5 volt half sine wave input to the nand gates (Motorola MC 846P).

These shape the pulse into the proper square wave for the monostable multivibrator (Motorola MC 851P). External timing capacitors and resistor allow one to select delays ranging from 0.01 to 0.8 seconds in the triggering pulses. This delay helps to position the first pulse on the grand maximum of the interferogram when one-sided runs are desired. The phase error in the fourier transform is thereby minimized. The counter (Motorola MC 839P) allows selection of the desired frequency range to be scanned during the experiment. For example, the divide-by-four output will sample the interferogram every 32 microns producing a spectrum from 0 to 156 cm^{-1}. The "set" button on the counter is used for one-sided interferograms. The button is depressed until just prior to scanning through the central maximum in the interferogram. When the button is released the next incoming pulse clears all the flip-flops in the counter and triggers the digital system.

The Brookdeal model 450 preamplifier has good noise characteristics for the signals of about 50 microvolt strength from our bolometer. The output from the Brookdeal model 411 phase sensitive detector is monitored with a pen recorder simultaneously as the digital system is recording readings. Any excessive noise on the interferogram is readily apparent and the run may be discontinued. The Non-Linear Systems model X-2 digital voltmeter has resolution of 10^{-4} which is adequate for our best signal-to-noise ratio of 1000 on the

0 to 625 cm^{-1} spectra. The trigger circuit and transformer in the phase shifter provide electrical isolation of the signal measuring apparatus from the interferometer.

b) Sample Growth and Preparation

The zinc dopant for the crystals studied was prepared by reacting zinc oxide with an excess of hydrofluoric acid and drying at 110°C.

$$ZnO + 2HF \rightarrow ZnF_2 + H_2O$$

The zinc fluoride and manganese fluoride powder (from Alfa Inorganics) were placed in a thinwall (0.4 mm) Ultra Purity[12] graphite crucible which was placed in a Stockbarger furnace containing HF atmosphere. It was heated above the 872°C melting point of ZnF_2 for about an hour before lowering the temperature to begin crystal growth. This ensures both the manganese and zinc fluoride are molten and an excess zinc concentration at the top of the resulting crystal does not occur. Any zinc oxide remaining in the prepared dopant would be readily converted to the fluoride by the HF gas at the high temperature in the furnace.

The melt was lowered out of the hot zone at a rate of 2.5 mm per hour. The crystals were cooled to room temperature over a period of 15 hours. This does not always eliminate the thermal strains. When attempting to cut the crystals to sample holder size they invariably cracked. However, good quality crystals about 0.5 cm thick could be removed from the boule although they were not large enough to orient them along a desired direction.

Neutron activation and atomic absorption techniques, however showed only a trace of zinc impurity in these crystals even with 4% ZnF_2 present in the melt.

Pure samples of MnF_2 were obtained from Alfa Inorganic and Optovac.

Because manganese fluoride has many transverse optical phonon frequencies above 150 cm^{-1}, thick crystals are almost opaque above this frequency due to restrahl absorption. This is beneficial for the low freqency (25 to 85 cm^{-1}) measurements where every second point in the interferogram may be sampled without introducing higher frequency errors into the spectrum. To provide appreciable transmission in the range 150 to 350 cm^{-1} the crystals were ground to 0.5 mm thickness with a one or two degree wedge to eliminate most interference fringes. These were glued with GE 7031 varnish into a thick washer hollowed out on one side. The varnish is transparent to far infrared radiation and is a good thermal conductor at low temperatures. The washer ensures the crystals do not crack due to the mechanical and thermal strains caused by the sample holder.

CHAPTER III

THEORY

Manganese fluoride crystallizes in a tetragonal structure (body-centred if we ignore the positions of the fluorines) with the manganese ions occupying the centre and corners of the unit cell. The manganese ions are in a $^6S_{5/2}$ state and the spins order antiferromagnetically along the c-axis below the Neél temperature of 67.3°K. The absence of orbital angular momentum for the manganese simplifies the theoretical treatment of the magnetic excitations since the higher excited states lie some 2 eV[7] away and thus the normal states of the system are pure magnons.

The magnon dispersion relation has been described adequately by Low et al[4] using exchange coupling up to third nearest neighbours and an anisotropy field.

$$\hbar\omega = 2Sz_2|J_2|(1+0.073/2S)[(1+\varepsilon)^2-\gamma^2]^{1/2}$$

where

$$\varepsilon = (H_A/2Sz_2|J_2|)-(2z_1J_1/z_2J_2)\sin^2(\tfrac{1}{2}cq_z)$$
$$- (z_3J_3/z_2J_2)[\sin^2(\tfrac{1}{2}aq_x)+\sin^2(\tfrac{1}{2}aq_y)]$$
$$\gamma = \cos(\tfrac{1}{2}aq_x)\cos(\tfrac{1}{2}aq_y)\cos(\tfrac{1}{2}cq_z)$$

S is the spin on the manganese ion

J_n is the exchange integral between an ion and its z_n nth nearest neighbours.

and H_A is the effective anisotropy field.

Using this dispersion relation Allen et al[3] have constructed a single magnon density of states in MnF_2 which exhibits sharp features at various points at the zone boundary. They explain the electric-dipole-induced two-magnon absorption via an effective spin Hamiltonian involving the electric field of the incident radiation and the spin operators of the system. Loudon[7] also develops a closely related formalism to account for the observed strength and shape of the absorption. The interaction is only between nearest neighbours and is of the form:

$$H = \sum_{i,j} \{AE\sigma^{y}_{ij} + A^{*}E^{y}\sigma^{x}_{ij} + BE^{z}\sigma^{x}\sigma^{y}_{ij}\sigma^{z}_{ij}\}S^{-}_{i}S^{+}_{j}$$

$$+ \text{ complex conjugate } + S^{z}_{i}S^{z}_{j} \text{ term}$$

where A and B are constants, E^{α} are components of the electric field, and σ_{ij} is a vector whose components have the value $\pm$ 1 determined by

$$\sigma^{\alpha}_{ij} = \mathrm{sign}(\underline{r}_{j} - \underline{r}_{i})_{\alpha} \quad ; \alpha = x,y,z$$

The term which gives rise to the selection rules for multiple magnon processes is the $\sum_{ij} S^{-}_{i}S^{+}_{j}$ term. Thus we can use the Holstein-Primakoff transformation of S^{-}_{i} and S^{+}_{j} to boson creation and annihilation operators a* and a:

$$S^{-}_{i} = (2S)^{1/2}\ a^{*}_{i}\ (1 - a^{*}_{i}a_{i}/2S)^{1/2}$$

$$S^{+}_{j} = (2S)^{1/2}\ a^{*}_{j}\ (1 - a^{*}_{j}a_{j}/2S)^{1/2}$$

$$S^{z}_{i} = S - a^{*}_{i}a_{i}$$

$$S^{z}_{j} = -S + a^{*}_{j}a_{j}$$

Then

$$S_i^- S_j^+ = 2S\ a_i^* \,(1-a_i^* a_i/2S)^{1/2}\ a_j^* \,(1-a_j^* a_j/2S)^{1/2}$$

$$= 2S\ a_i^* \,(1-a_i^* a_i/4S - \ldots)\ a_j^* \,(1-a_j^* a_j/4S - \ldots)$$

$$= 2S\ (a_i^* a_j^* - a_i^* a_j^* a_j^* a_j/4S - a_i^* a_i^* a_i a_j^*/4S)$$

retaining terms only up to fourth order in the operators. A further transformation to spin wave variables:

$$a_i = N^{-1/2} \sum_k e^{-ik\cdot x_i}\, b_k \qquad a_i^* = N^{-1/2} \sum_k e^{ik\cdot x_i}\, b_k^*$$

$$a_j = N^{-1/2} \sum_k e^{ik\cdot x_j}\, c_k \qquad a_j^* = N^{-1/2} \sum_k e^{-ik\cdot x_j}\, c_k^*$$

(where N is the number of atoms on a sublattice.)

gives

$$S_i^- S_j^+ = \frac{2S}{N} \sum_{k_1 k_2} e^{ik_1\cdot x_i}\, b_{k_1}^*\ e^{-ik_2\cdot x_j}\, c_{k_2}^*$$

$$- \frac{1}{2N^2} \sum_{k_1 k_2 k_3 k_4} e^{ik_1\cdot x_i}\, b_{k_1}^*\ e^{-ik_2\cdot x_j}\, c_{k_2}^*\ e^{-ik_3\cdot x_j}\, c_{k_3}^*\ e^{ik_4\cdot x_j}\, c_{k_4}$$

$$- \frac{1}{2N^2} \sum_{k_1 k_2 k_3 k_4} e^{ik_1\cdot x_i}\, b_{k_1}^*\ e^{ik_2\cdot x_i}\, b_{k_2}^*\ e^{-ik_3\cdot x_i}\, b_{k_3}\ e^{-ik_4\cdot x_j}\, c_{k_4}^*$$

The indices i and j refer to nearest neighbours on different sublattices and we can replace x_j by $x_i + \delta$ where δ is the vector joining atom at i to the neighbours at j.

Then

$$\sum_{i,j} S_i^- S_j^+ = \sum_{i,\delta} \Big[\frac{2S}{N} \sum_{k_1 k_2} e^{i(k_1-k_2)\cdot x_i} \; e^{-ik_2\cdot\delta} \; b_{k_1}^* \; c_{k_2}^*$$

$$- \frac{1}{2N^2} \sum_{k_1 k_2 k_3 k_4} e^{i(k_1-k_2-k_3+k_4)\cdot x_i} \; e^{-i(k_2+k_3-k_4)\cdot\delta} \; b_{k_1}^* \; c_{k_2}^* \; c_{k_3}^* \; c_{k_4}$$

$$- \frac{1}{2N^2} \sum_{k_1 k_2 k_3 k_4} e^{i(k_1+k_2-k_3-k_4)\cdot x_i} \; e^{-ik_4\cdot\delta} b_{k_1}^* \, b_{k_2}^* \, b_{k_3} c_{k_4}^* \Big]$$

$$= 2Sz \sum_{k_1 k_2} \delta(k_1-k_2) \; \gamma_{k_2} \; b_{k_1}^* \; c_{k_2}^*$$

$$- \frac{z}{2N} \sum_{k_1 k_2 k_3 k_4} \delta(k_1-k_2-k_3+k_4) \; \gamma_{k_2+k_3-k_4} \; b_{k_1}^* \; c_{k_2}^* \; c_{k_3}^* \; c_{k_4}$$

$$- \frac{z}{2N} \sum_{k_1 k_2 k_3 k_4} \delta(k_1+k_2-k_3-k_4) \; \gamma_{k_4} \; b_{k_1}^* \; b_{k_2}^* \; b_{k_3} \; c_{k_4}^*$$

$$= 2Sz \sum_{k} \gamma_k \; b_k^* \; c_k^*$$

$$- \frac{z}{2N} \sum_{k_1 k_2 k_3 k_4} [\delta(k_1-k_2-k_3+k_4) \; \gamma_{k_2+k_3-k_4} \; b_{k_1}^* \; c_{k_2}^* \; c_{k_3}^* \; c_{k_4}$$

$$+ \delta(k_1+k_2-k_3-k_4) \; \gamma_{k_4} \; b_{k_1}^* \; b_{k_2}^* \; b_{k_3} \; c_{k_4}^*]$$

where $$\gamma_k = z^{-1} \sum_{\delta} e^{ik\cdot\delta} = \gamma_{-k}$$

over the z nearest neighbours and assuming a centre of symmetry.

The first term in the expansion leads to the well known two-magnon absorption. The second and third terms are four-magnon processes. Expanding the H-P transformation to still higher orders will lead to six,-eight-, etc magnon scattering. The complex conjugate term ($S_i^+S_j^-$) and the term conserving the total number of magnons ($S_i^zS_j^z$) give similar results, except that $S_i^zS_j^z$ cannot be expanded beyond four-magnon processes.

Of note is that the four-magnon terms involve the creation of 3 magnons of different k vector and the destruction of a magnon with another k vector with the restriction that the vectors total zero according to the delta functions. The fact that there is a magnon destruction operator implies that the process will be highly temperature dependent. The lowest energy magnon is at k=0 (AFMR) and has a thermal energy of about 12°K. At liquid helium temperature (4.2°K) there will not be an appreciable number of magnons to be destroyed since the number of thermal magnons excited in the system would vary according to the Planck distribution

$$<n> = \frac{1}{e^{\hbar\omega/kT} - 1}$$

the factor being ∿0.05 at 4.2°K. Also, the density of states for magnons is very small near k=0, rising to peaks near the zone boundary. The thermal energy of the zone boundary magnons is of the order of 70°K. Therefore, although the absorption due to four-magnon processes would increase with temperature, it would also broaden and shift toward lower frequencies. This is because of decreasing sublattice magnetization and that the captured magnon may have successively higher energy. One would expect the absorption to be most noticeable in the medium temperature range around 45°K.

The absorption would necessarily be much weaker than the two-magnon absorption because it is down by a factor of $(\frac{a^*a}{4S})^2$ from the two-magnon process. An estimate would be of the order of 1% of the two-magnon integrated intensity.

Phonon assisted dipole-exchange interactions as suggested by Halley[10] would perhaps increase the strength of these processes. A term of the form b*c*c*c would have its greatest contribution from the creation of magnons near the zone boundary where the density of states is a maximum. An absorption somewhere around 150 cm^{-1} could be expected and it would shift to lower frequencies and grow in intensity with increasing temperature as the number of magnons which could be destroyed increased.

Manganese fluoride has 6 atoms per unit cell giving rise to 18 phonon branches, 15 optical and 3 acoustic. Thus the phonon spectrum would necessarily be complex and near a phonon absorption one could expect a modification of the exchange parameter in the Heisenberg hamiltonian tending to increase the strength of the magnon processes. In fact, as will be seen in the results of the experiments, a strong traverse optical phonon absorption occurs at 158 cm^{-1} almost where one might expect a four-magnon absorption to occur.

CHAPTER IV

EXPERIMENTAL RESULTS AND DISCUSSION

(a) Low Frequency Data (25 to 85 cm^{-1})

Figures 7 through 9 show the absorption in the region 25 to 85 cm^{-1} of two different crystals of MnF_2 which were doped with ZnF_2 (1 and 4%) in the melt prior to growth. Any absorptions in pure MnF_2 have been eliminated by dividing the spectra of the home-grown crystals by the spectrum of a pure crystal obtained from Alfa Inorganics. All crystals were 3.3 ± 0.2 mm thick. Absorption peaks at 31.1 cm^{-1} and 63.5 cm^{-1} are present in both the spectrum of crystal A (1% ZnF_2 in the melt) and of B(4% ZnF_2 in the melt). The absorption at 63.5 cm^{-1} varies from 20% in crystal B to about 5% in A. The integrated intensity under the peaks also is in a 4:1 ratio. However, the absorption at 31.1 cm^{-1} has roughly the same strength in both crystals. Comparison with spectra from the pure MnF_2 confirms that this peak is not caused by filters or by some other impurity in the pure crystal.

To determine if either of these peaks are caused by magnetic excitations a magnetic field was applied to crystal B where both absorptions are stronger. Figure 9 is the spectrum with an applied field of 58 kilogauss. It is not significantly different from the zero field spectrum (figure 8). The ratio of five runs at zero field to five runs with a 58 kilogauss

Figure 7

Transmission spectrum of sample A of MnF_2 3.3. mm. thick, with zero applied magnetic field. Impurity absorptions are observable at 31.1 and 63.5 cm^{-1}.

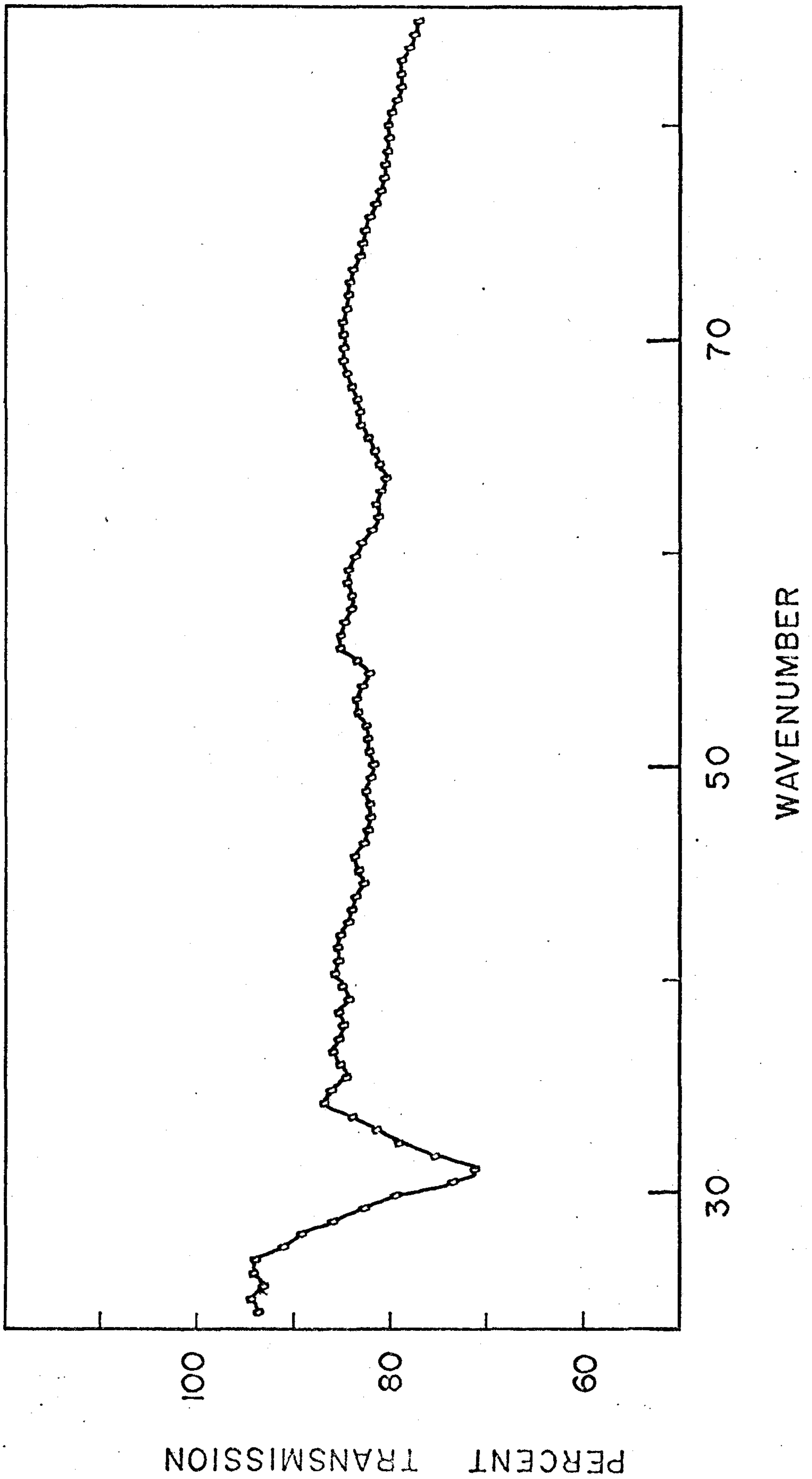
PERCENT TRANSMISSION
100
80
60
WAVENUMBER
30
50
70

Figure 8

Transmission spectrum of sample B of MnF_2, 3.3 ± 0.2 mm. thick, with zero applied magnetic field. The absorptions at 31.1 and 63.5 cm^{-1} are stronger than in sample #1 (Figure 7). Also there appears to be a broad weak absorption between 42 and 58 cm^{-1}.

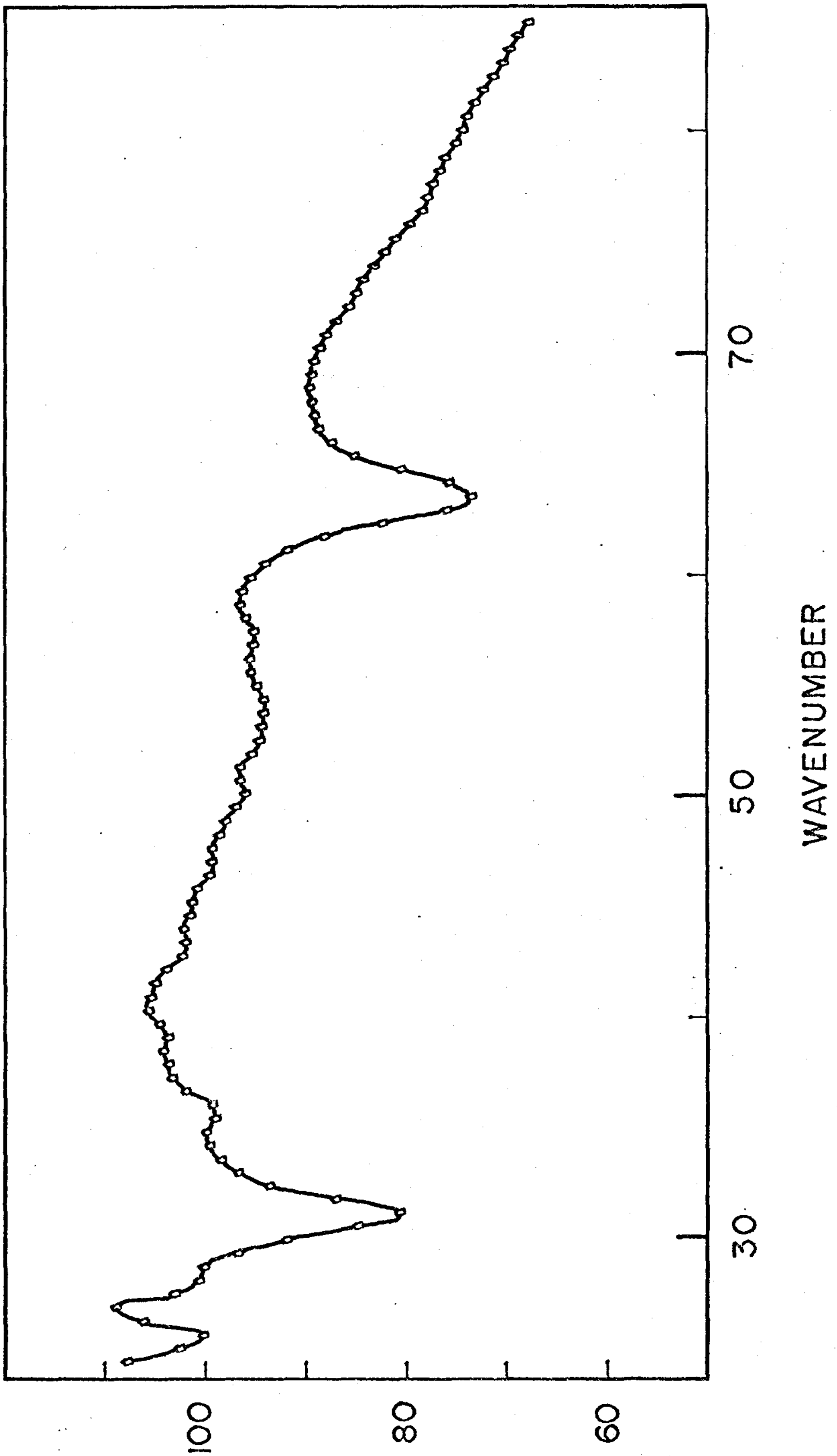
PERCENT TRANSMISSION
100
80
60
WAVENUMBER
30
50
70

Figure 9

Transmission spectrum of sample B of MnF_2 with a 58 kilogauss applied field.

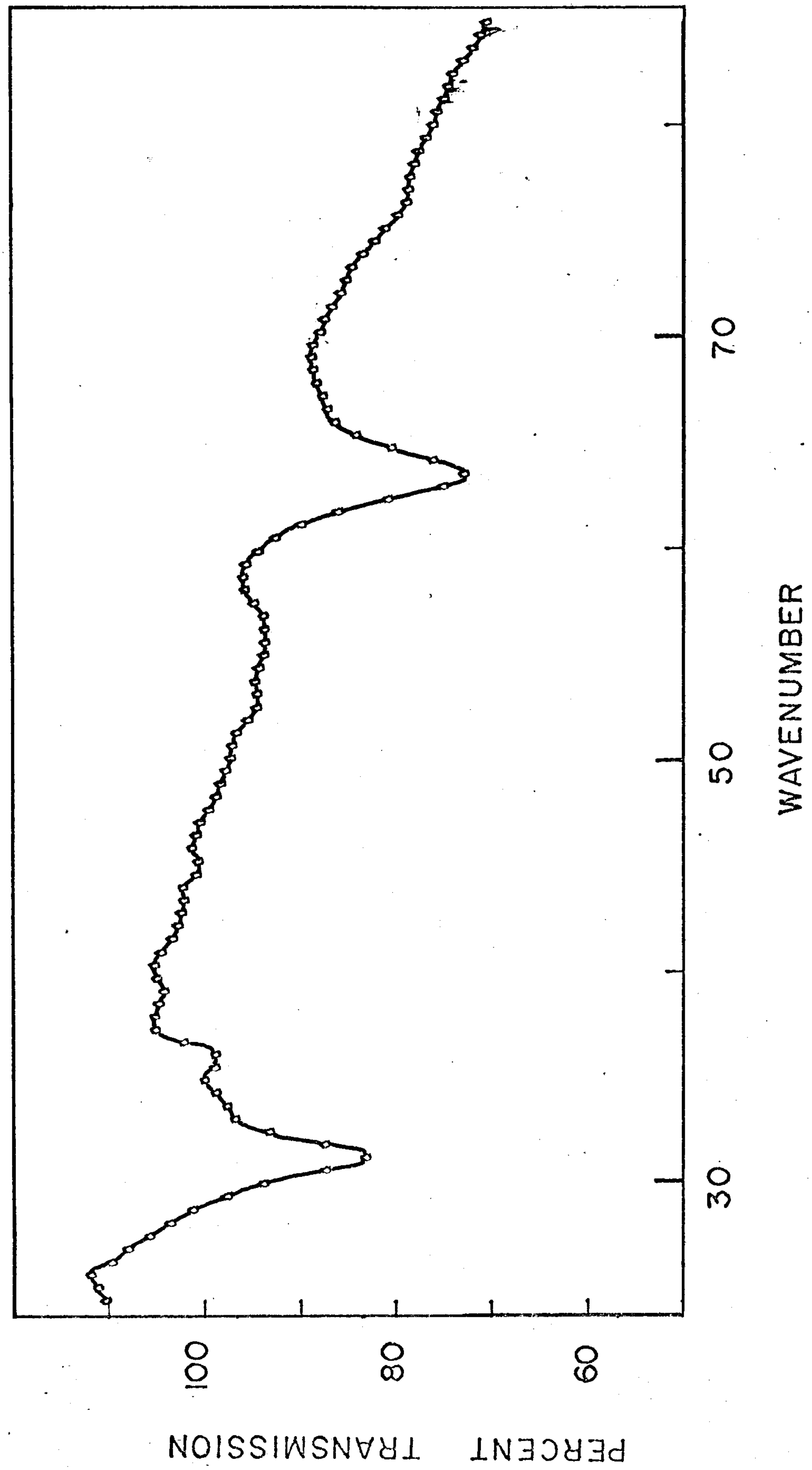
PERCENT TRANSMISSION
100
80
60
30
50
70
WAVENUMBER

Figure 10

The ratio of figures 8 and 9. The peak at 26 cm^{-1} is thought to be caused by noise. If the splitting of the 63.5 cm^{-1} peak is as shown by the arrows, the g value for the peak is about 0.45. One would expect a g value of 2 for manganese.

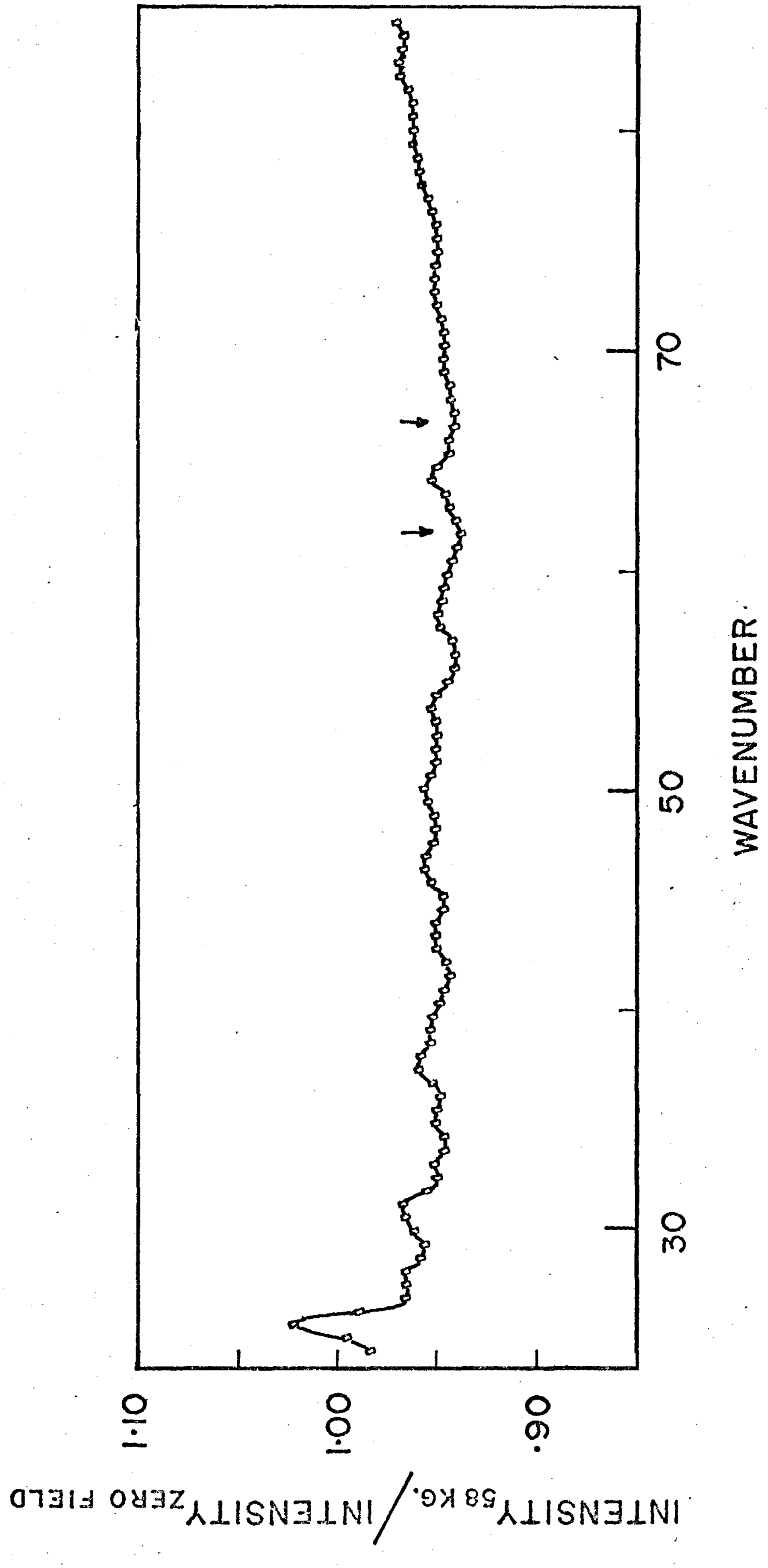
1·10
1·00
·90
INTENSITY58 KG./INTENSITYZERO FIELD
30
50
70
WAVENUMBER

Figure 11

Low noise ratio of sample B of MnF_2 with 58 kilogauss applied field to zero applied field in order to determine any magnetic effects to the broad peak between 42 and 58 cm^{-1} (figure 8). The experiment would have detected a shift for $g \geq 0.90$. No shift is observed.

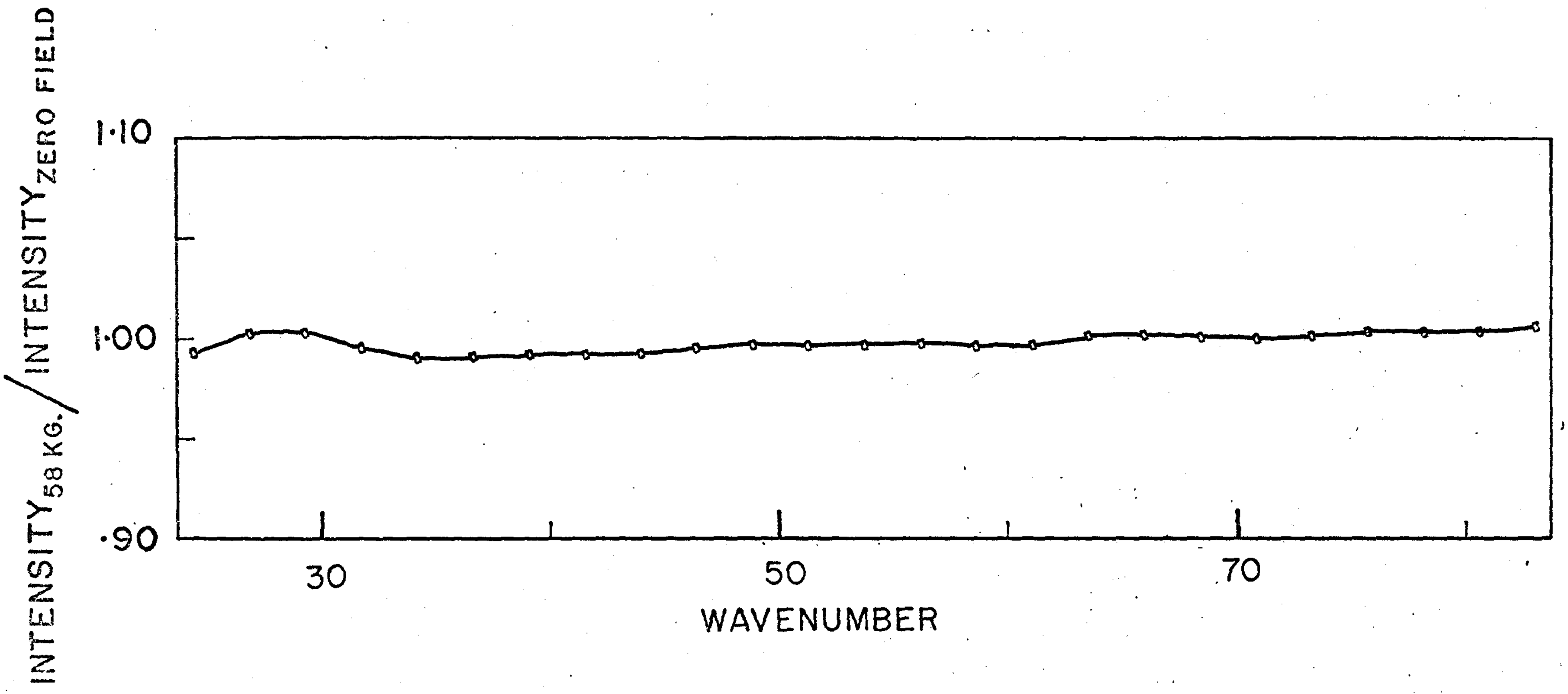
INTENSITY$_{58\ KG.}$/INTENSITY$_{ZERO\ FIELD}$
1·10
1·00
·90
30
50
70
WAVENUMBER

field is given in figure 10. Averaging ten runs reduced the noise on the spectrum to about 1.5% RMS about the 70 cm^{-1} region. The g value for manganese is 2 and the expected shift of the peaks would be about 4 cm^{-1} if they were caused by magnons. Assuming the deviations about the mean value of the ratio indicated by the arrows is caused by a splitting of the 63.5 cm^{-1} peak, the calculated g factor for the peak is about 0.45.

There appears to be a broad weak absorption in crystal B between 44 and 58 cm^{-1} in figure 8. The one magnon density of states is highest around this range. In order to ascertain whether this broad peak is an impurity-induced one-magnon absorption, forty low resolution run (4.9 cm^{-1}) were done; twenty at zero field and twenty at 58 kilogauss field. Figure 11 is the ratio of the spectra obtained. The RMS noise on the ratio is less than 0.5% over the range 35 to 85 cm^{-1}. An applied magnetic field removes the degeneracy of the dispersion curves in manganese fluoride. Two identical one-magnon densities of states would result, shifted up and down in frequency by the appropriate $g\mu_\beta H$ value. Here g is the gyromagnetic ratio of manganese, μ_β is the Bohr magneton, and H is the applied external field. The expected splitting for a g of 2 would be about 8 cm^{-1} in this case. A shift in the absorption for a $g \geq 0.9$ would have been detected by the experiment. The ratio is unity throughout the range of interest and within the limit of the noise in the experiment it is not possible to determine if it is indeed a one-magnon absorption.

Johnson and Nethercot[13] obtained a value of about 6 cm^{-2} for the integrated intensity of the antiferromagnetic resonance in pure MnF_2. One would expect the induced one-magnon absorption in a doped crystal to approach this value as the concentration is increased to 100%. The AFMR should broaden as well in a doped crystal. The absorption in question in figure 8 has an integrated intensity of 1 cm^{-2}. This is about a factor of 3 higher than could be expected even for a 4% doped crystal. Svensson et al[14] were not able to detect any broadening of the AFMR in 5% zinc doped MnF_2. From this we can conclude that the strength of the induced one-magnon absorption in this experiment would have been less than 1% of the strength of the AFMR. This could not be resolved from the noise on the spectrum.

Svensson et al[14] do indicate a lowering of the frequency of the zone boundary magnons by about 5% in the zinc doped crystal and in addition a broad resonance at 3/4 of the zone boundary wave vector in both <100> and <001> directions. Changes in the magnon density of states corresponding to the perturbed dispersion curves would possibly be noticeable in the two-magnon absorption occuring around 110 cm^{-1}. Unfortunately the experiments were performed using a beamsplitter giving virtually zero intensity at 100 cm^{-1} and a comparison of the pure crystal and our sample was not possible.

The fact that the observed peaks in the spectra are independent of applied magnetic field leads to the conclusion that the absorptions are caused by phonons. A rigid ion calculation[15] of the phonon density of states in MnF_2 shows maxima at 35 and 70 cm^{-1} (5 cm^{-1} resolution). These maxima arise from the first acoustic branch of the dispersion curves. An impurity in a crystal destroys the symmetry and the $k=0$ radiation can couple to phonons along this branch out to the zone boundary. Thus peaks in the density of states would be seen as absorptions in the spectrum. The phonons are created via an electric dipole interaction and would be more prominent than magnons which are due to a magnetic dipole interaction.

(b) High Frequency Data (50 to 350 cm^{-1})

Pure crystals of MnF_2 were studied in this region. Figure 12 is the spectrum of an Optovac crystal, 0.017 mm thick, oriented such that the electric field of the incident radiation is both parallel and perpendicular to the c-axis of the sample ($E \parallel c$ and $E \perp c$). Absorption in the spectrum occur at 100, 171, 210, 260, and around 330 cm^{-1}. The broad peak at 100 cm^{-1} is the two-magnon absorption reported by Allen et al.[3] An explanation of the other peaks will be given later.

Figure 13(a) through (f) give the spectra of a randomly oriented, 0.5 mm thick crystal of MnF_2 from Alfa Inorganics for the temperature range 11 to 85°K. Random orientation would exhibit all the general features of various possible polarizations. The centroid of the two-magnon

Figure 12

Spectrum of pure MnF_2 crystal (Optovac), 0.17 mm thick with the c-axis in the plane of the sample.

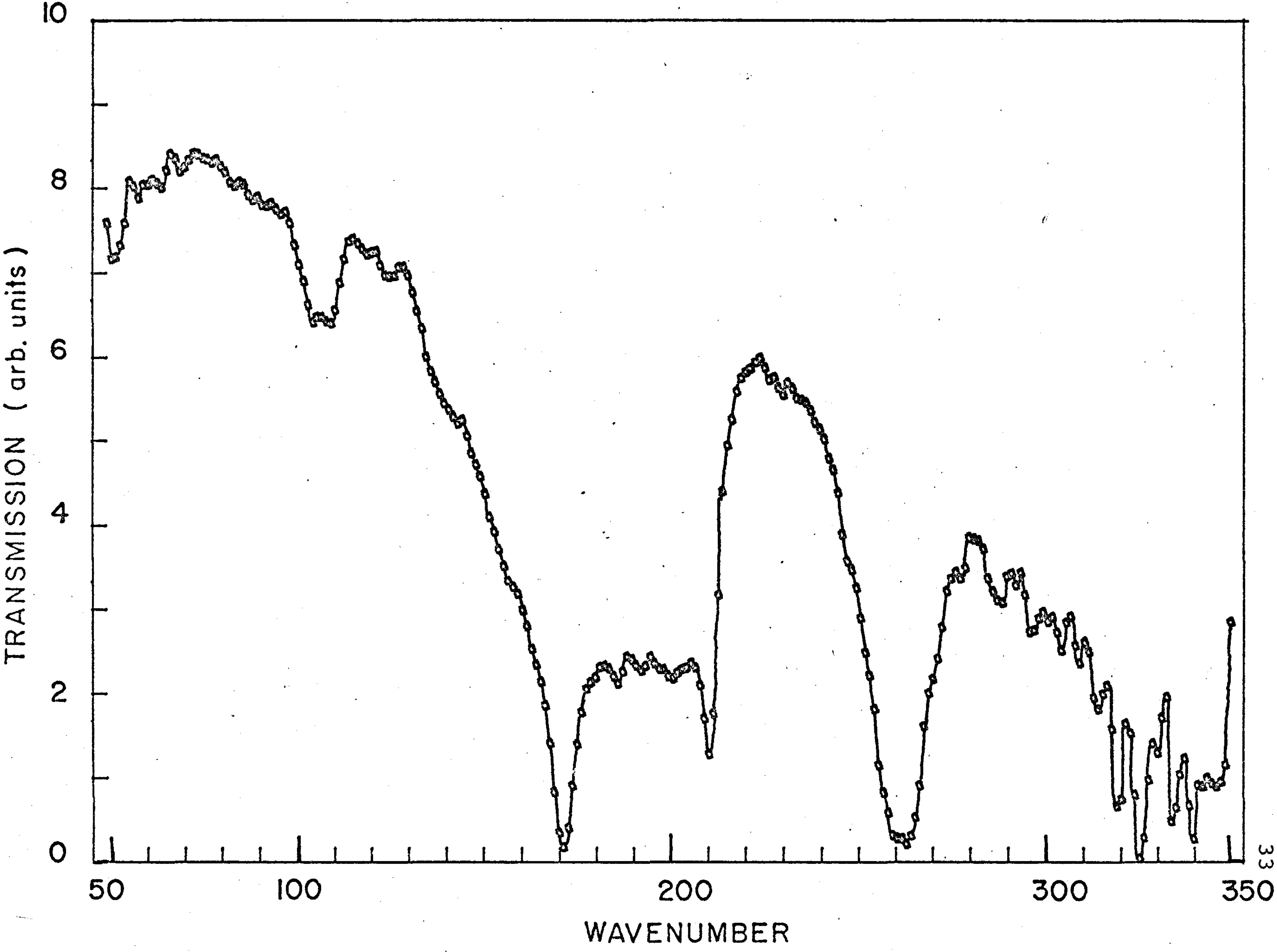
10
8
6
4
2
0
TRANSMISSION (arb. units)
50
100
200
300
350
WAVENUMBER

Figures 13(a) to (f)

Spectra of a randomly oriented crystal of pure MnF_2 (Alfa), 0.5 mm thick, at various temperatures. The two-magnon absorption shifts from 107 cm^{-1} at 11°K to 80 cm^{-1} at 61°K. The peaks at 171 and 210 cm^{-1} do not change their position.

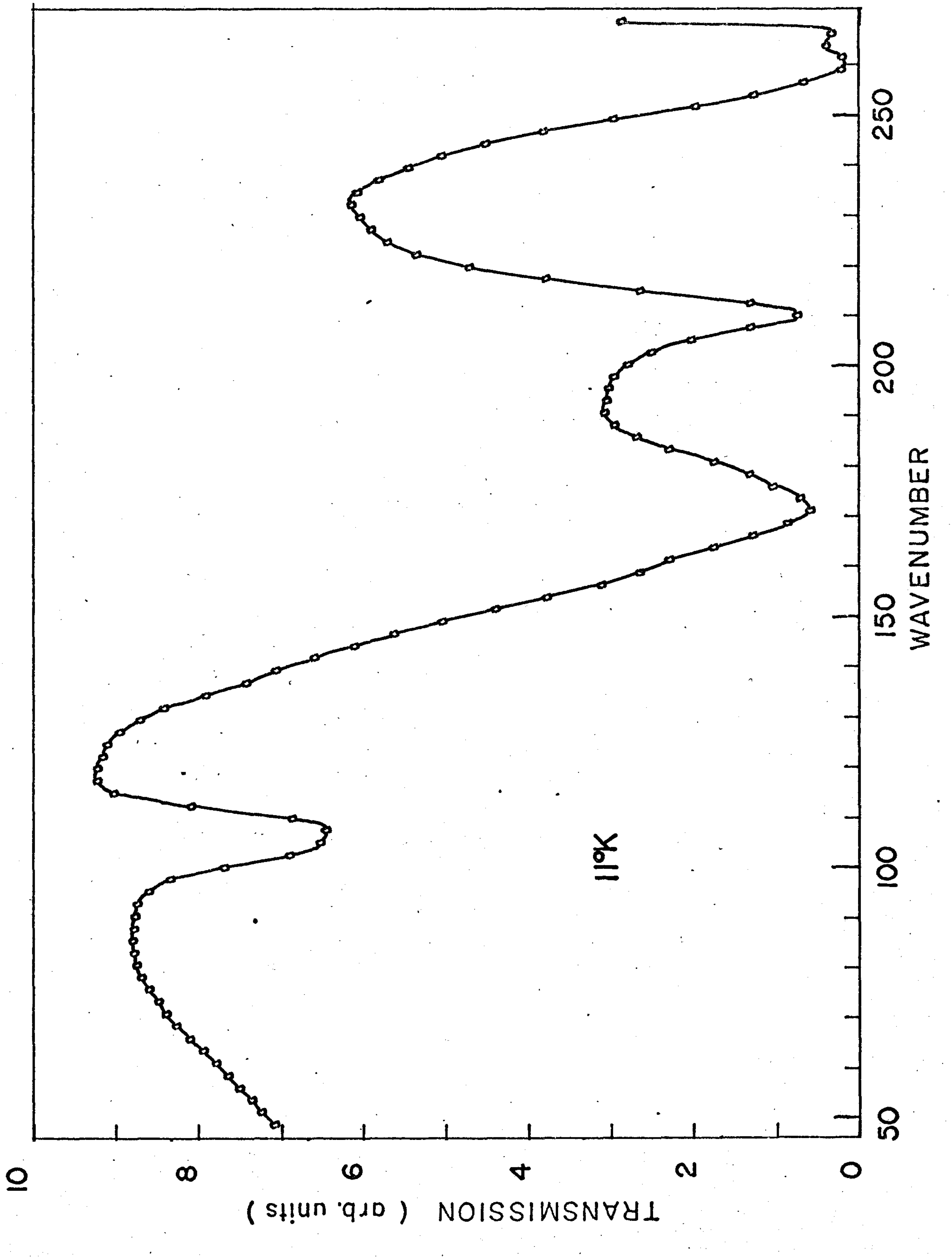
TRANSMISSION (arb. units)
0
2
4
6
8
10
WAVENUMBER
50
100
150
200
250
11°K

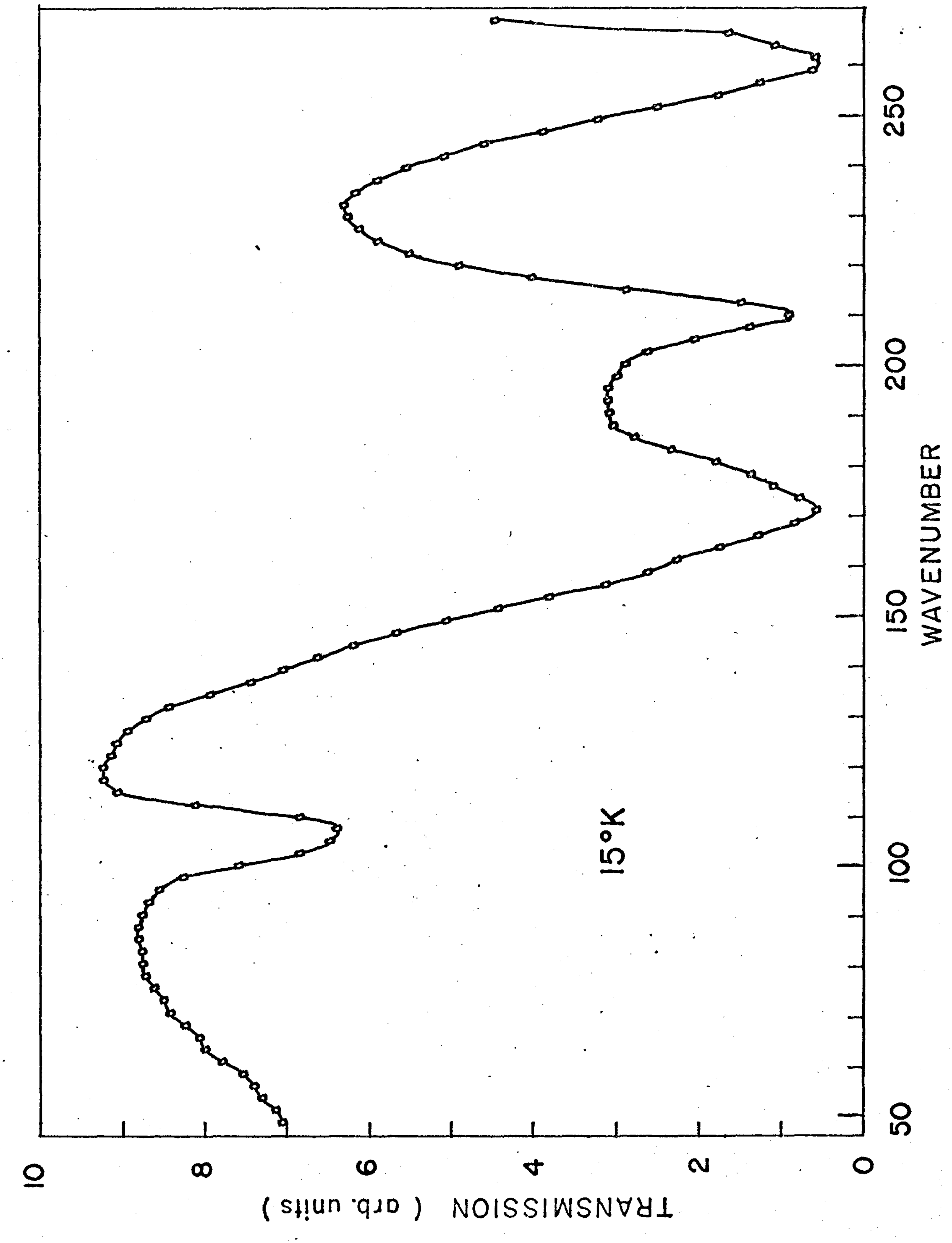
15°K
TRANSMISSION (arb. units)
0
2
4
6
8
10
WAVENUMBER
50
100
150
200
250

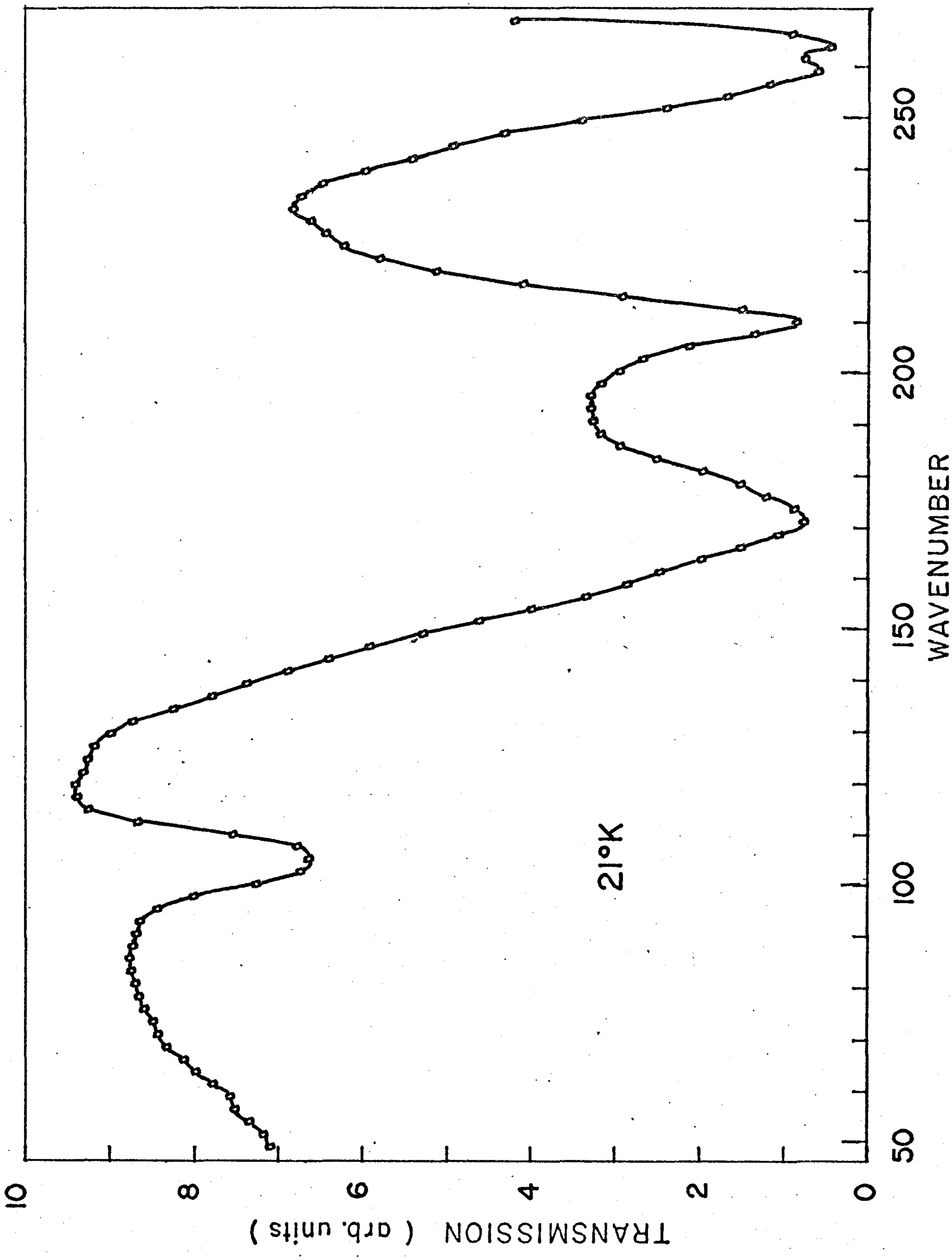
21°K
WAVENUMBER
50
100
150
200
250
TRANSMISSION (arb. units)
0
2
4
6
8
10

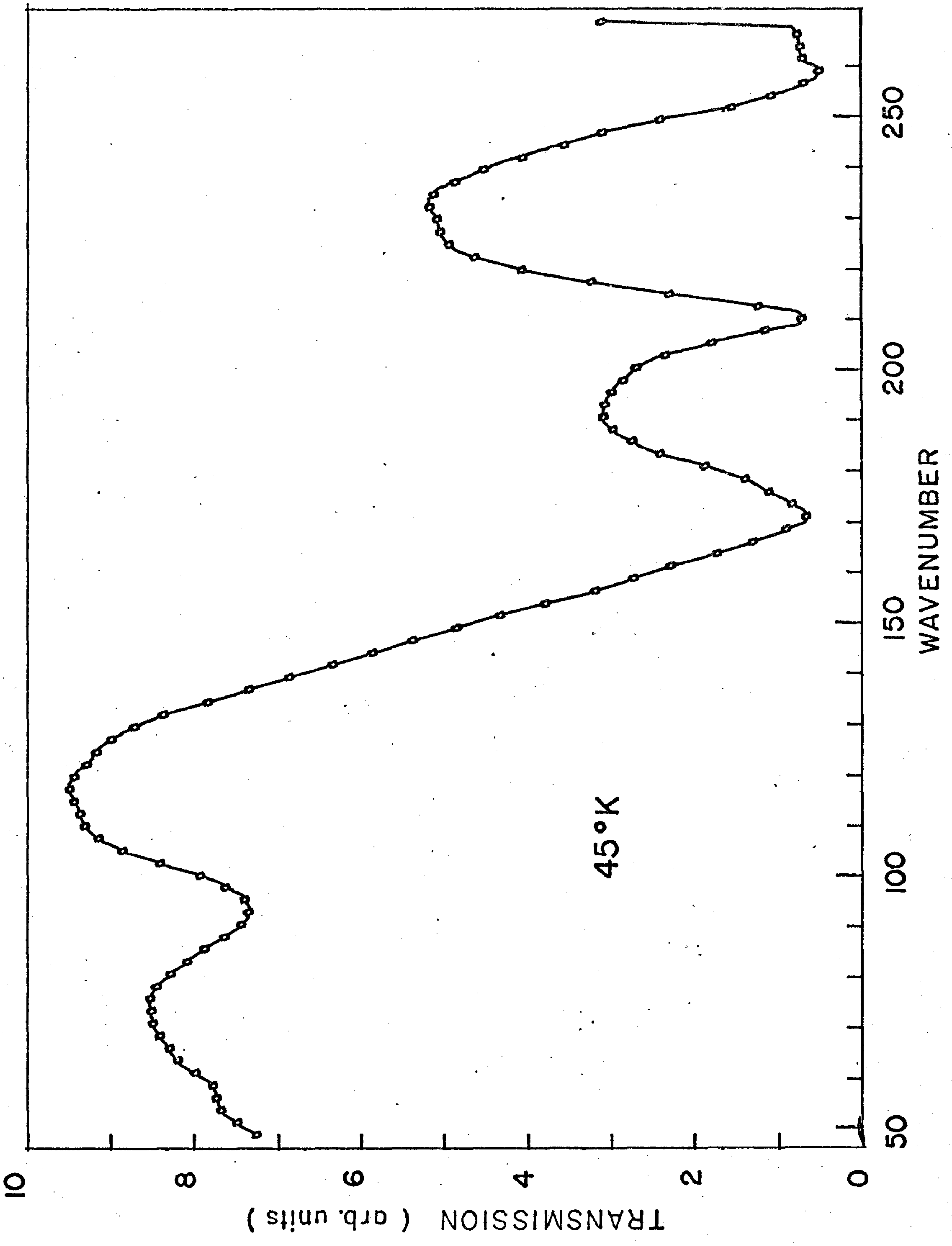
45°K
TRANSMISSION (arb. units)
10
8
6
4
2
0
WAVENUMBER
50
100
150
200
250

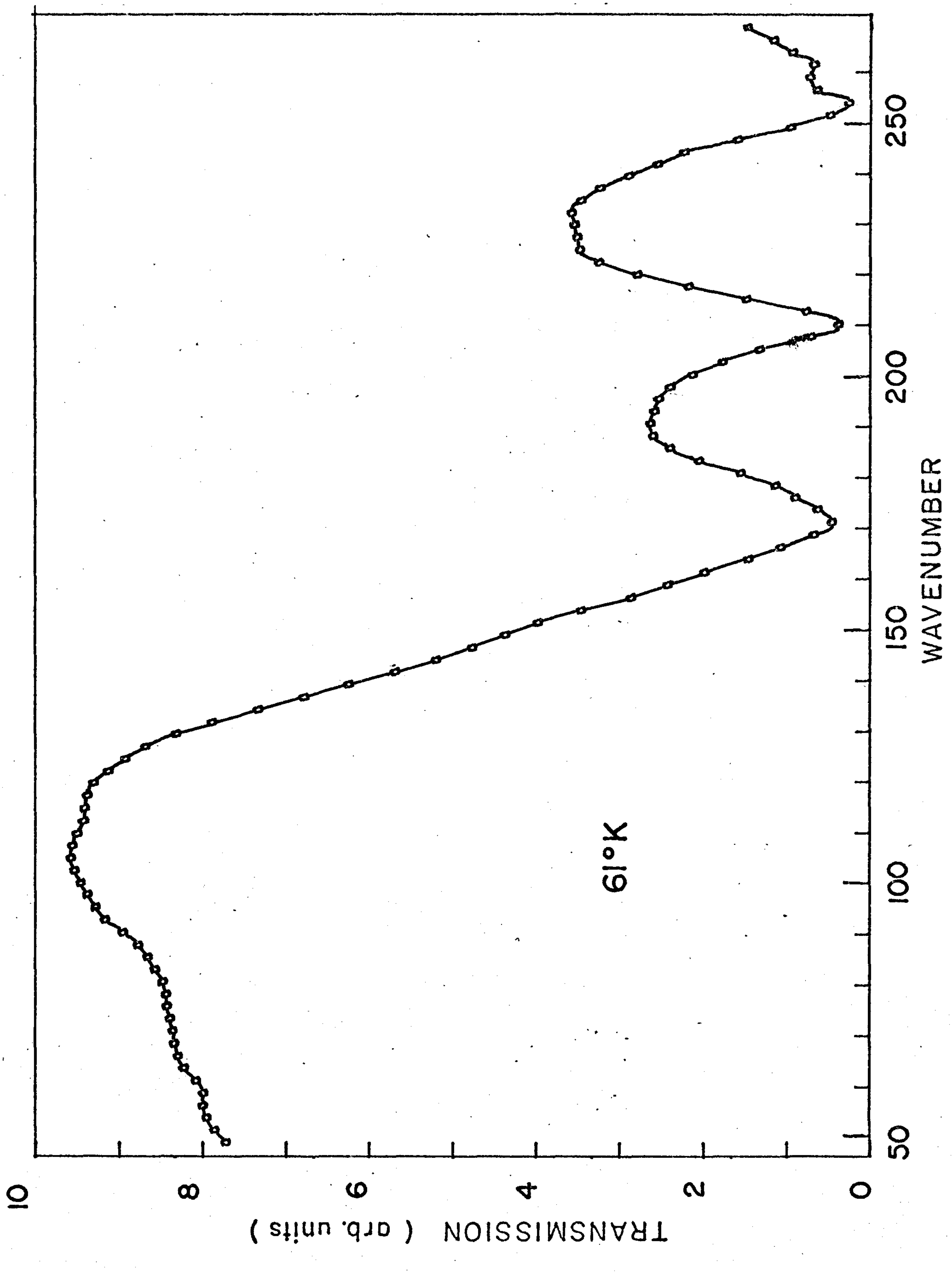
61°K
TRANSMISSION (arb. units)
WAVENUMBER
0
2
4
6
8
10
50
100
150
200
250

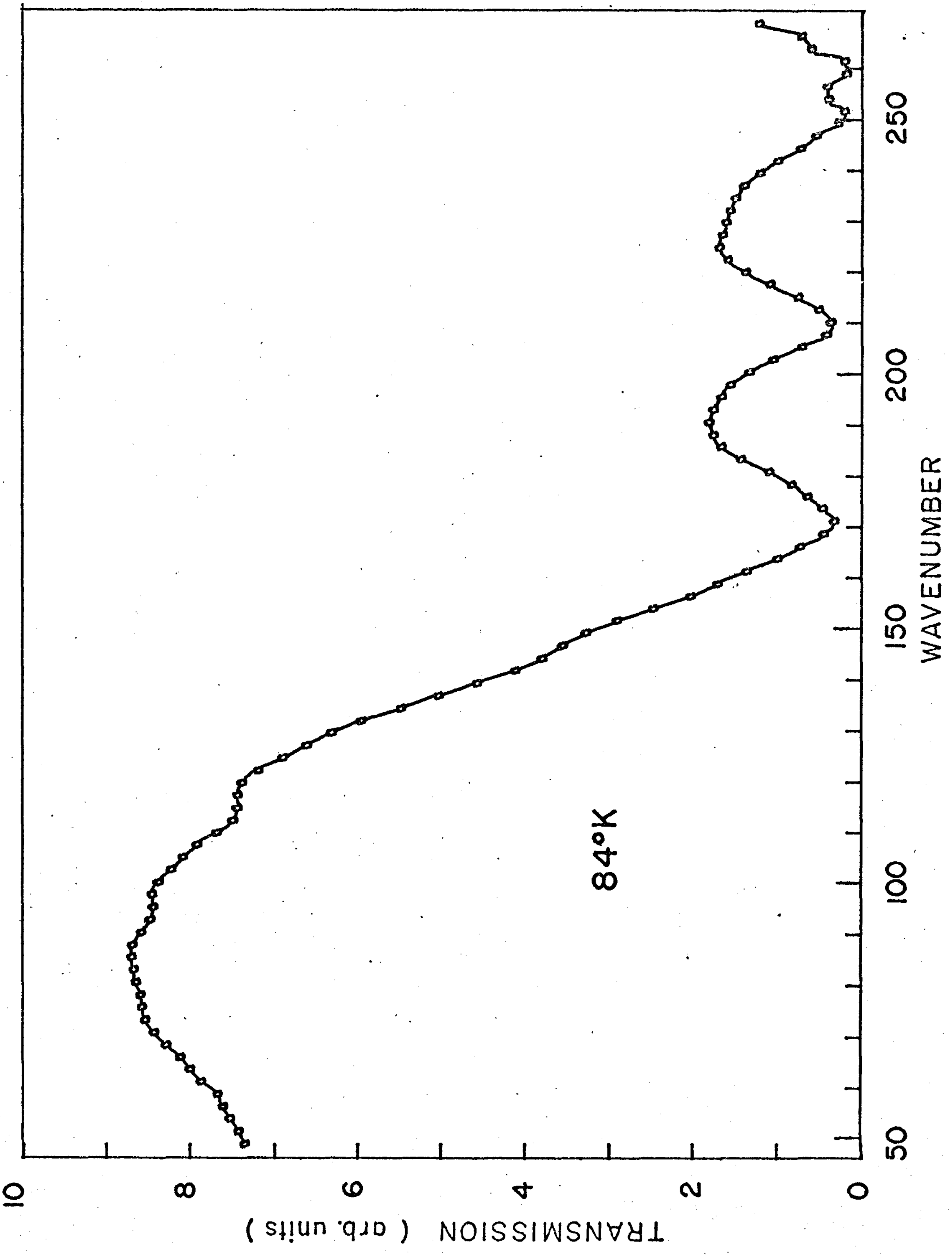
84°K
TRANSMISSION (arb. units)
0
2
4
6
8
10
WAVENUMBER
50
100
150
200
250

absorption shifts from 107 cm^{-1} at 11°K to about 83 cm^{-1} at 61°K. It cannot be detected at 84°K (above the Neél point). No similar shift or boradening of the peaks at 171 and 210 cm^{-1} is observed. The possibility that these peaks are due to higher order magnon processes is therefore eliminated.

The relative frequency of the two-magnon centroid, the zone boundary magnon in the <001> direction as measured by Okazaki et al[16], by inelastic neutron scattering, and the value of the Brillouin function for S=5/2 as given by Smart[17] are plotted against reduced temperature in figure 14. The Brillouin function describes the temperature dependence of the sublattice magnetization in the molecular field theory. Both the zone boundary magnon frequency and the two-magnon centroid are somewhat higher than the sublattice magnetization. Measurements by Heller[18] of the F^{19} zero-field NMR frequency in MnF_2 also show that the molecular field approximation is too low at higher temperatures. Presumably the discrepancy is due to magnon-magnon interactions and the onset of short range order in particular for the two-magnon absorption. Both effects are ignored by the molecular field theory.

If, as has been suggested by Shapiro[19], magnon absorptions other than those involving an even number of magnons exists, the application of an external magnetic field could be expected to alter the spectrum. Figure 15 and 16 are high resolution (0.16 cm^{-1}) spectra of pure MnF_2 with zero and 57 kilogauss applied magnetic field respectively. As expected, the two

Figure 14

Comparison of the relative frequencies of the two-magnon centroid, the zone-boundary magnon (band mode) in the <001> direction[16], and the brillouin brillouin function for S=5/2[17], versus temperature. The 4.2°K value for the two-magnon centroid is taken from the data of figure 15. Both the band mode and two-magnon absorption are considerably higher than the molecular field theory sublattice magnetization (Brillouin function with S=5/2).

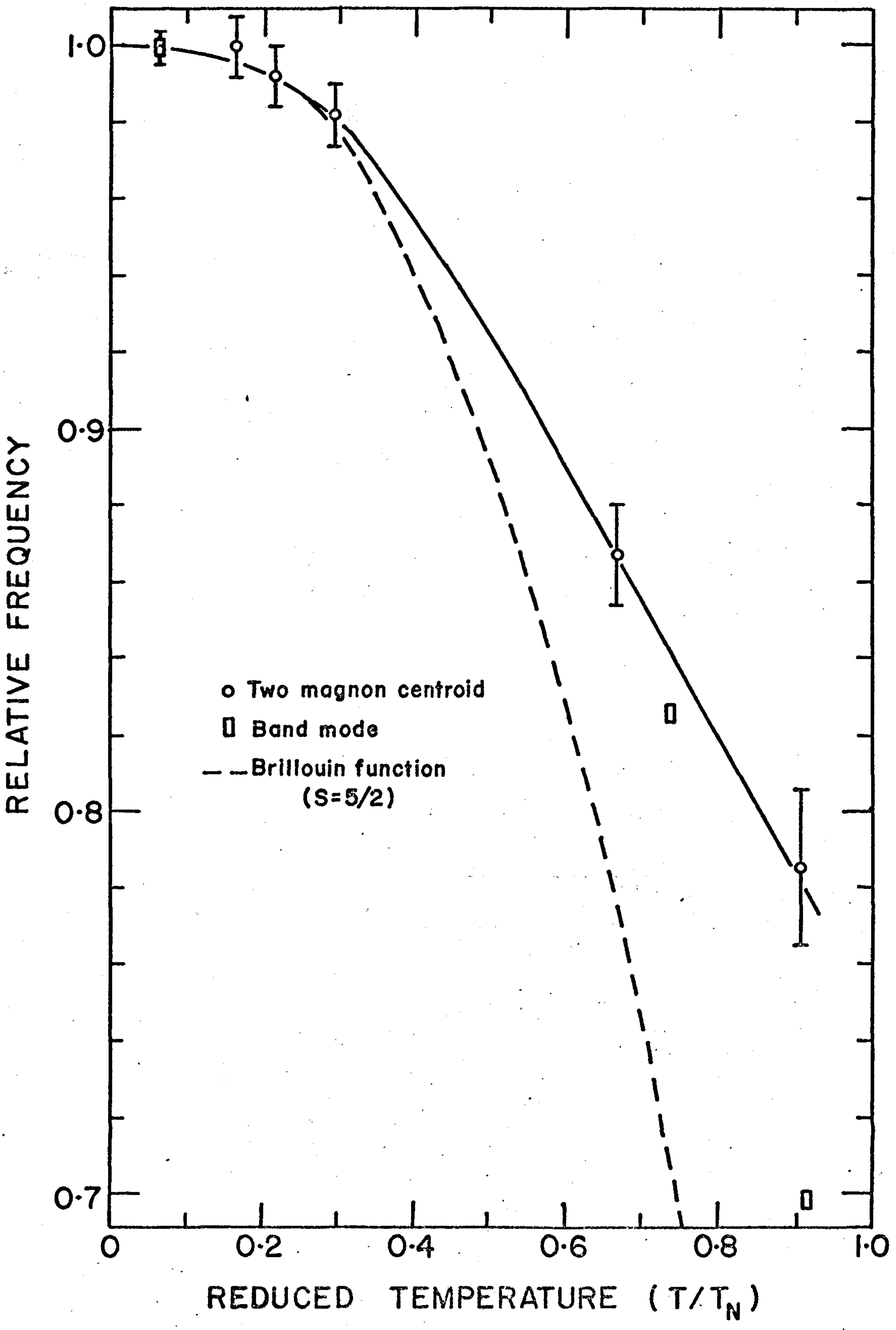
1·0
0·9
0·8
0·7
RELATIVE FREQUENCY
0
0·2
0·4
0·6
0·8
1·0
REDUCED TEMPERATURE (T/T_N)
○ Two magnon centroid
▯ Band mode
– – Brillouin function
(S=5/2)

magnon absorption is unaffected. Also, the peaks at 170.9 and 210.6 cm^{-1} appear identical for both zero and 57 kilogauss field. If there is any shift of the peaks it is less than 0.61 cm^{-1} corresponding to a $g \leq 0.23$. Odd multiple magnon processes do not appear to cause these absorptions.

To identify the true nature of these absorptions experiments were performed with 0.5 mm thick slices of the Alfa crystal cut with the c-axis in the plane of the sample ($E \perp C$ and $E \parallel C$) and perpendicular to the plane of the sample ($E \perp C$). The results are shown in figures 17 and 18. Figure 17, $E \perp C$, displays zero transmission between 158 and 210 cm^{-1} and weaker absorptions between 250 and 258 cm^{-1} and from 320 cm^{-1} to the high frequency limit. Beyond this point the intensity of incoming radiation is small and the noise level on the spectrum is too large for an acceptable analysis. The two-magnon absorption is not visible because it is very weak in this orientation.

In figure 18, $E \perp$ and $\parallel C$, the two-magnon absorption at 110 cm^{-1} is causes almost entirely by $E \parallel C$. No radiation having $E \perp C$ passes through the crystal in the range 158 to 210 cm^{-1} as evidenced by the abrupt change in transmission at 158 cm^{-1}. About 50% of the light is transmitted to 210 cm^{-1}. The absorptions at 171 and 210 cm^{-1} are thus caused by radiation having $E \parallel C$. Absorption bands from 250 to 268 cm^{-1} and from 310 cm^{-1} to the limit of the spectrum are also present.

Parisot[20] has performed reflection measurements on MnF_2

Figure 15

High resolution (.61 cm^{-1}) spectra of .5 mm slice of pure MnF_2 (Alfa) with the c-axis in the plane of the sample.

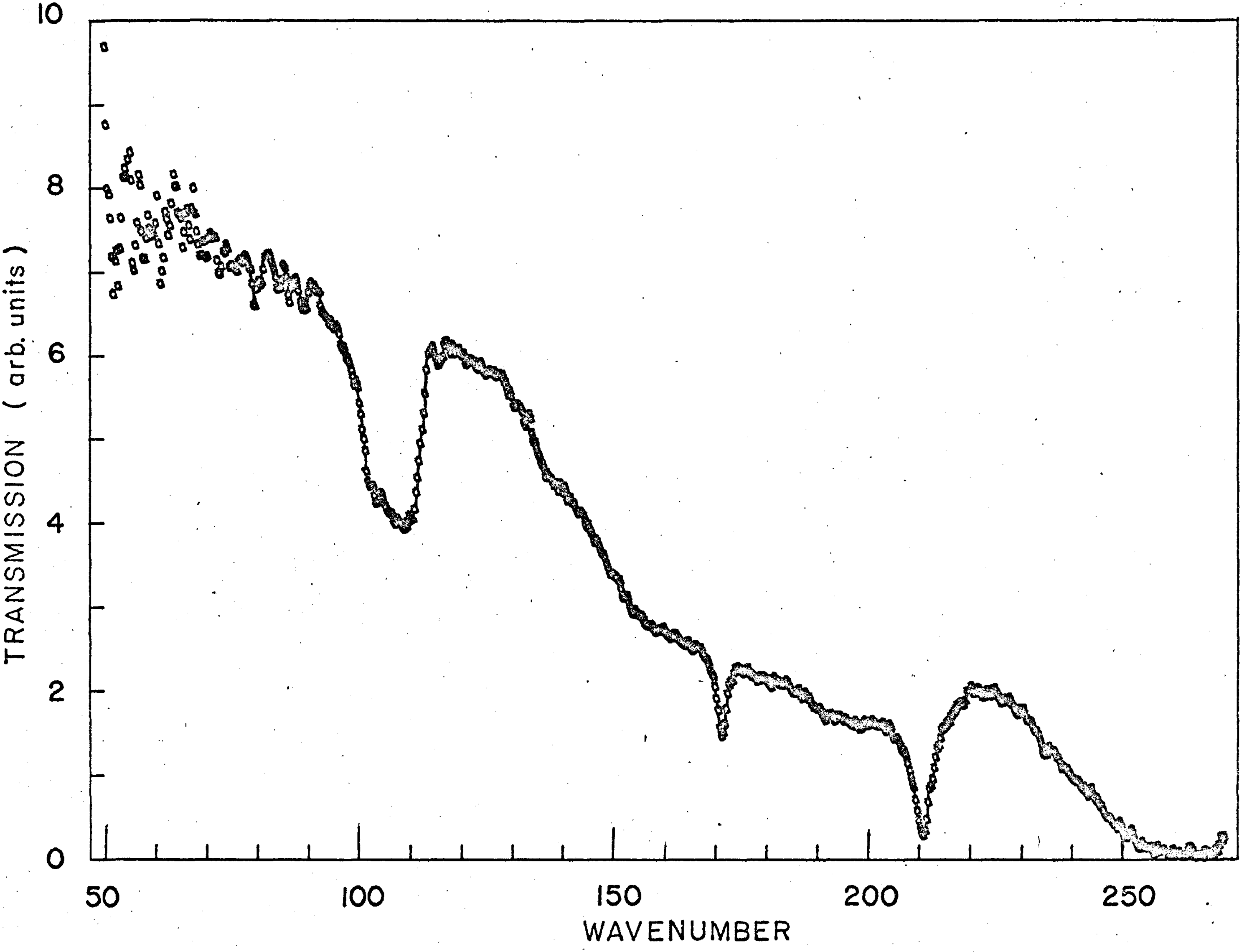
10
8
6
4
2
0
TRANSMISSION (arb. units)
50
100
150
200
250
WAVENUMBER

Figure 16

Spectrum of the sample of Figure 15 with an applied field of 57 kg. No shift of the peaks at 171 and 210 cm^{-1} can be detected.

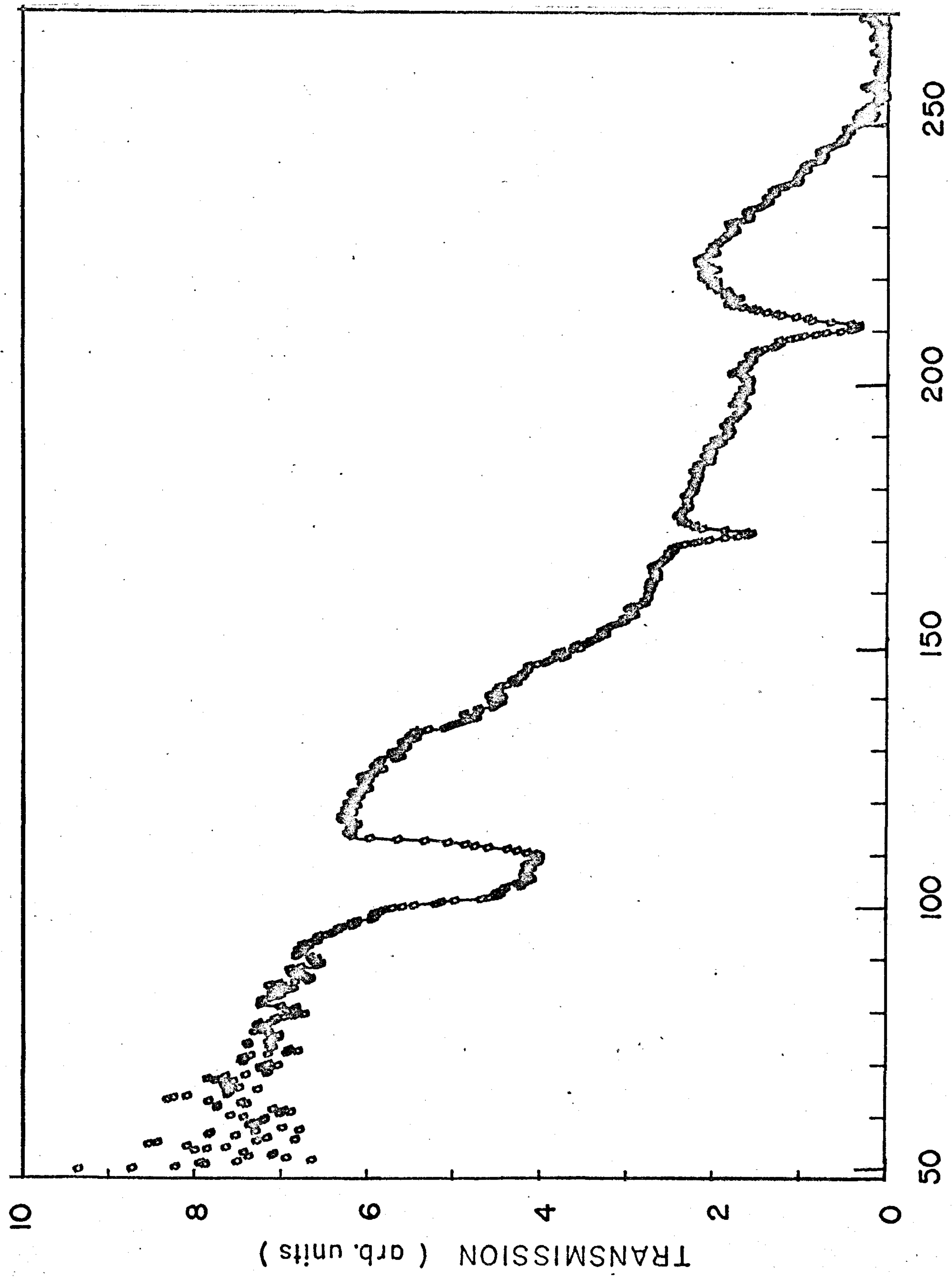
TRANSMISSION (arb. units)
0
2
4
6
8
10
WAVENUMBER
50
100
150
200
250

Figure 17

Pure MnF_2 (Alfa) .5 mm thick with the c-axis perpendicular to the plane of the sample.

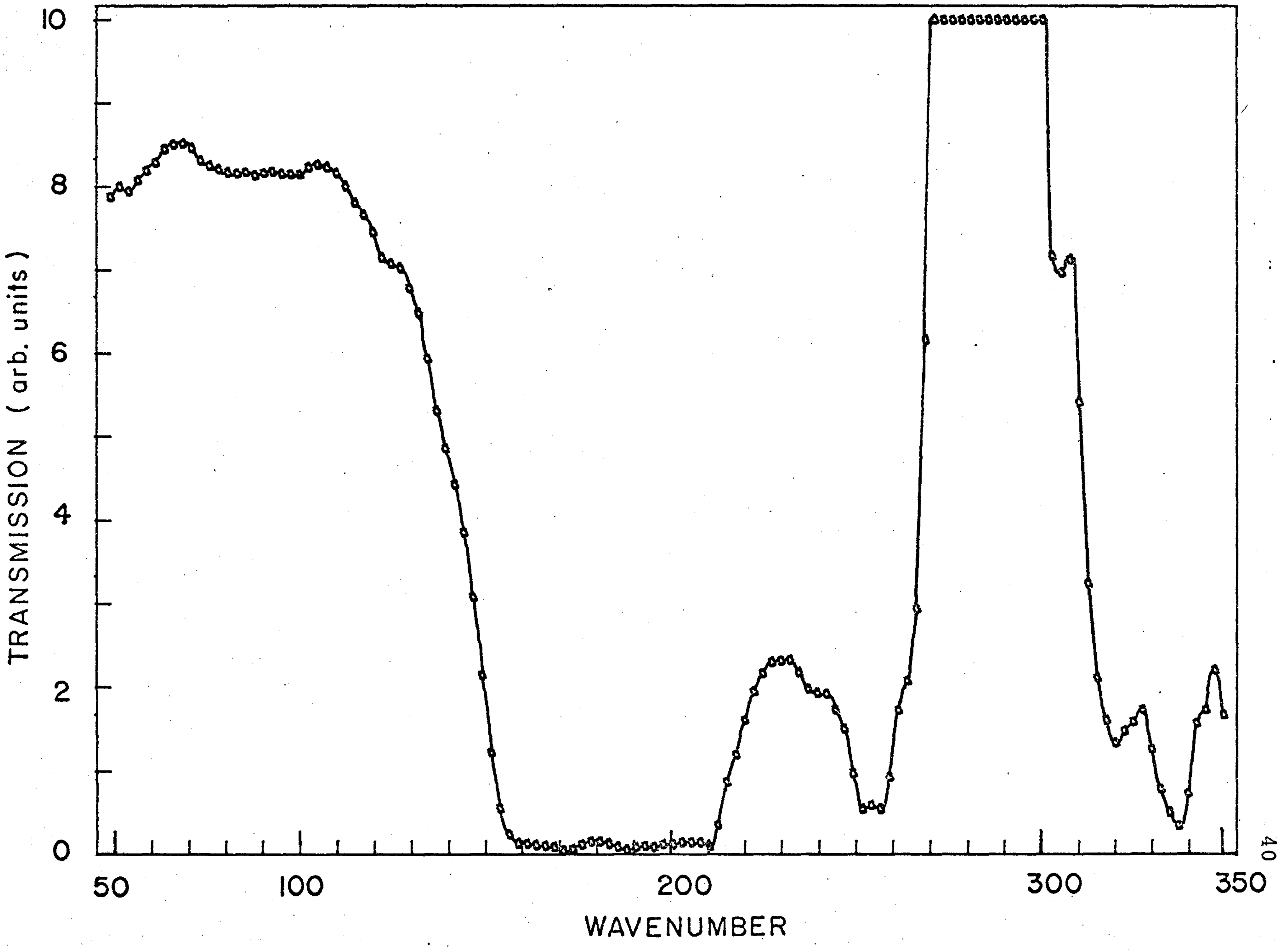
TRANSMISSION (arb. units)
10
8
6
4
2
0
50
100
200
300
350
WAVENUMBER

Figure 18

Pure MnF_2 (Alfa) .5 mm thick with the c-axis in the plane of the sample.

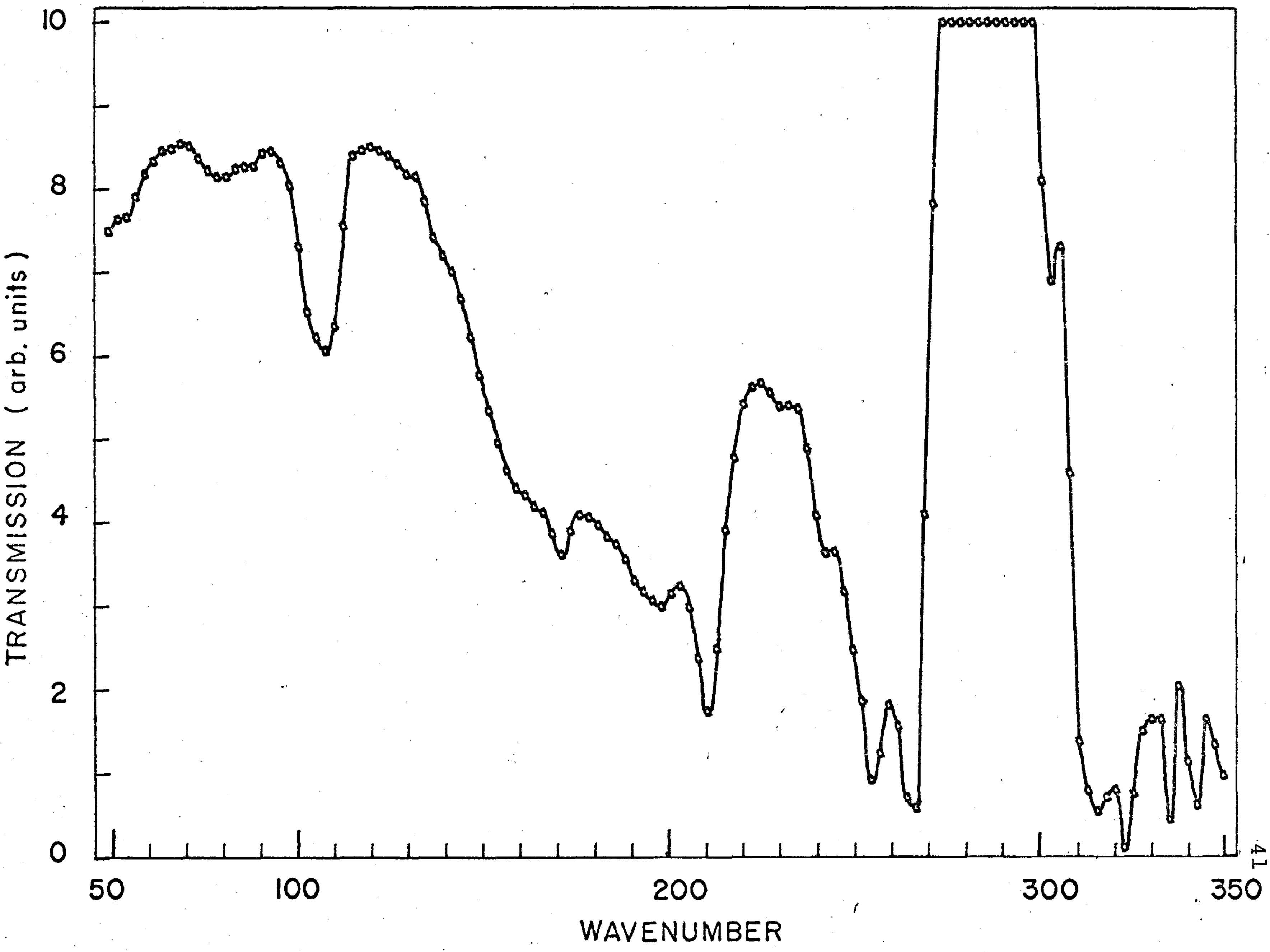
TRANSMISSION (arb. units)
0
2
4
6
8
10
WAVENUMBER
50
100
200
300
350

at room temperature. His results show a transverse optical phonon frequency of 158 cm^{-1} and a longitudinal optical phonon frequency of 210 cm^{-1} for the $E \perp C$ orientation. No modes for light $E \perp C$ are allowed to propogate through the crystal between the above frequencies. The present experiments agree with his results. In addition, for $E \perp C$ there is another transverse optical phonon at 255 cm^{-1} and a longitudinal at 260 cm^{-1}, and for $E \parallel C$ a transverse phonon at 295 cm^{-1} and longitudinal at 520 cm^{-1}. For both crystal alignments in the present work the spectra exhibit only weak transmission in the range 250 to 268 cm^{-1} and beyond 310 cm^{-1}. Again, the agreement with Parisot's work is good but the noise on the spectra does not allow the phonon frequencies to be determined more accurately.

Unless there are other infrared active zero wave vector frequencies in manganese fluoride for $E \parallel C$, no absorptions should appear between 158 and 210 cm^{-1} in figure 18. We must assume the specimens used in this experiment contain impurities which induce the absorptions at 171 and 210 cm^{-1}. The spectrum of the 0.17 mm thick Optovac crystal (figure 12) has the same general shape as the spectrum of the 0.5 mm thick Alfa crystal (figure 18). However, the absorption at 171 cm^{-1} is much stronger in the Optovac crystal than in the thicker Alfa crystal. The 210 cm^{-1} absorption is weaker in the Optovac sample. The orientation of these samples were verified accurate to at least 2° by means of crossed polaroids and x-ray diffraction experiments. The different absorption strengths are not caused by different alignment in the sample holder. Other spectra which were obtained from pure crystals grown by us showed similar variations in the absorptions at 171 and 210 cm^{-1}. They definitely appear to be caused by impurities.

The previously mentioned rigid ion model calculation[15] of the density of phonon states produces a large maximum at 170 cm^{-1}. The impurity induced absorption at 171 cm^{-1} in the spectra would correspond to this large density of states. The absorption at 210 cm^{-1} may be a coupling to the zero wave vector longitudinal optical phonon by means of the impurities in the crystal.

CHAPTER V

CONCLUSIONS AND PROPOSALS

The impurity induced one-magnon absorption could not be detected in this experiment. However, it would be an excellent means for determining the nature of the one-magnon density of states. Critical points which are observed in the two-magnon absorption are affected by magnon-magnon interactions which are not well understood theoretically. The use of thicker samples of better quality and a less noisy detector would be required to progress further.

The multiple magnon absorptions which were shown to be theoretically possible could not be resolved in this experiment as well. There are some difficulties in observing them which perhaps are not easily overcome. One cannot perform the experiments on thicker crystals due to the broadened restrahl absorptions. The presence of the many phonon absorptions above 150 cm^{-1} also would tend to obscure magnon processes in thin crystals. Careful temperature dependent measurement from 15 to 40°K around the150 cm^{-1} region would seem to be the best way of detecting such processes.

At the present time there has not been sufficient neutron work done on the phonons in MnF_2 to develop an accurate theory for the lattice dynamics. The phonons which were observed in this experiment agree fairly well with a rough calculation of the density of states and other optical reflection measurements. Some further progress could be made through the studies of crystals with known impurity concentrations but without a good model to fit the results this seems inadvisable.

References

1. R. Weber, Journal of Applied Physics <u>40</u>, 995 (1969).
2. W.J.L. Buyers, R.A. Cowley, T.M. Holden, and R.W.H. Stevenson, Journal of Applied Physics <u>39</u>, 1118 (1968).
3. S.J. Allen, R. Loudon, and P.L. Richards, Phys. Rev. Letters, <u>16</u>, 463 (1966).
4. G.G. Low, A. Okazaki, R.W.H. Stevenson, and K.C. Turberfield, Journal of Applied Physics <u>35</u>, 998 (1964).
5. O. Nikotin, P.A. Lindgard, and O.W. Dietrich, Jour. Phys. C. (Solid State Physics) Ser. 2 Vol. 2, 1168 (1969).
6. K.C. Turberfield, A. Okazaki, and R.W.H. Stevenson, Proc. Phys. Soc. <u>85</u>, 743 (1965).
7. R. Loudon, Adv. Phys. <u>17</u>, 243 (1968).
8. R.J. Elliott, and M.F. Thorpe, Jour. Phys. C. (Solid State Phys.) Ser. 2 Vol. 2, 1630 (1969).
9. T. Moriya, Journal of Applied Physics <u>39</u>, 1042 (1968).
10. J.W. Halley, Phys. Rev. <u>154</u>, 458 (1967).
11. A.J. Tumber, M.Sc. Thesis, McMaster University, (1968).
12. Technical Service Laboratories, Toronto, Ontario. Density grade UF-4S.
13. F.M. Johnson and A.H. Nethercot, Phys. Rev. <u>114</u>, 705 (1959).
14. E.C. Svensson, T.M. Holden, W.J.L. Buyers, and R.A. Cowley, Solid State Comm. <u>7</u>, 1693 (1969).
15. R.O.W. Kuehnel, McMaster University, Private communication.
16. A. Okazaki, K.C. Turberfield, and R.W.H. Stevenson, Phys. Letters <u>8</u>, 9 (1964).
17. J.S. Smart, Effective Field Theories of Magnetism (Philadelphia and London: W.B. Saunders, 1966).

18. P. Heller, Phys. Rev. 146, 403 (1966).

19. M.M. Shapiro and R. Stevenson, Journal of Applied Physics 40, 989 (1969).

20. G. Parisot, C.R. Acad. Sc. Paris 265, 1192 (1967).